UNIVERSITY OF Southampton
School of Ocean and Earth Science

Wind and wave variability in re-analysis models and satellite measurements in the North Atlantic

RAY BELL

Master of Oceanography

Supervisors:

Dr. David Cromwell, Dr. Christine Gommenginger and

Prof. Meric Srokosz

SOES 6030: Msci Advanced Independent Research Project

May 2010

Word count: 15, 598

Acknowledgements

I would like to take this opportunity to thank my supervisors for making this project possible; David Cromwell for supplying me with the satellite data and his time spent advising me where to go with the project. Christine Gommenginger, for the regular discussions and helping me put results into context. Meric Srokosz, for his suggestions on the project and reading through early drafts. I would also like to thank Graham Quartly, Andrew Shaw, Craig Wallace and Paolo Cipollini for their help and allowing me permission to use their Matlab codes. To Ed, for breaking up the working day with basketball and the guys of Soton Uni Breakers. I would finally like to thank my Father Paul Bell and Mother Maureen Bell and for reading through early drafts and their continual support throughout the project.

Abstract

Winds and ocean surface gravity waves play a major role in many engineering and environmental issues both in the open ocean and in coastal zones. It is therefore essential to improve our knowledge on the spatial and temporal variability of the winds and the wave climate. This study aims at investigating this variability in the North Atlantic (66^{o}N-10^{o}S, 100^{o}W-10^{o}E) for the period 1992-2009, from ECMWF re-analysis models, ERA-40, the recently released ERA-Interim and new long-term calibrated gridded satellite altimeter datasets developed at NOCS. ERA-Interim gives larger maximum values of wind speed compared to ERA-40 for the time period September 1992 – August 2002, but shows similar results for the four first modes of the Empirical Orthogonal Functions (EOFs). Maximum significant wave height (swh) is also increased in ERA-Interim but still underestimated in comparison to TOPEX data (January 1993 – August 2002). The first EOF from ERA-Interim explains 30% of the variance whereas the first EOF from the TOPEX data explains 22% of the variability. The principal components are correlated against the climatic indices of the North Atlantic Oscillation (NAO) and the East Atlantic Pattern (EAP). The satellite data of ERS-2 + Envisat dataset (May 1995 – December 2008) gives the strongest correlations and showed the first EOF is related to the EAP and the second EOF to the NAO. The NAO has much less of an influence on the first EOF in comparison to the shorter TOPEX data, suggesting an increase in the EAP's influence on the dominant mode of variability or a decrease in the NAO's influence in recent years. Large differences are observed between the two models and the satellite data for wave period. The spatial patterns are different between the two models, with the first EOF for ERA-40 explaining 47% of the variance and the first EOF for ERA-Interim accounting for only 27% of the variance. This is reduced to 14% with the TOPEX data and gives a different spatial pattern. The TOPEX data also showed the first EOF to be explained by the EAP and the second EOF by the NAO. The TOPEX + Jason-1

dataset (May 1995 – December 2008) shows a decrease of the NAO's influence on the first EOF in recent times. The wind speed in the North Atlantic in observed to show teleconnections from the tropical Pacific by correlating the anomalies against the Multivariate ENSO Index anomalies, as an area of positive correlation with r = 0.3, which is statistically significant at the 95% level, in the western tropical North Atlantic with a lag of 4-6 months occurs. These teleconnections are also observed in swh and wave period.

Contents

1. Project outline

The aims of this study are:

- To observe, understand and quantify the seasonal, interannual and decadal variability of the wind speeds and wave climate of the wave model datasets; ERA-40 and ERA-Interim.

- To examine possible differences between ERA-40 and ERA-Interim wind and wave data, as well as differences between 10 day versus 35 day repeat cycle altimeter datasets.

- To see how the model data compare against satellite radar altimeter data from the TOPEX, Jason-1, ERS-2 and Envisat satellites, with methods such as Empirical Orthogonal Functions (EOFs) within the extended North Atlantic basin (66^{o}N-10^{o}S, 100^{o}W-10^{o}E).

- To obtain climate indices for the NAO, EAP and Multivariate ENSO index (MEI) and apply statistical tests, such as regression, to see if both the wave model data and satellite data is sensitive to the changing atmospheric conditions in the same way.

2. Introduction

Climatological data on wind and wave processes are useful in many areas of study. Knowledge of the wave climate is useful for engineering design (e.g. ships and offshore platforms), shipping routes, locating surface slicks and air-sea fluxes which influence carbon uptake and release from the ocean (Krogstad and Barstow, 1999; Tucker and Pitt, 2001).

Winds are important for the mixing of nutrients and plankton and influencing the level of primary production, which affects whole ecosystems. Long term results can help assess the estimates of ocean-based renewable energy resources (Mackay *et al*, 2010). Reports of an apparent increase in wave height in the North East Atlantic in recent years, have aroused considerable interest, especially the threat of more extreme wave conditions due to global warming proposed from in-situ results (Grevemeyer *et al*, 2000; Wang *et al*, 2009) and general circulation models (Wang *et al*, 2004).

The climatological wave parameters studied in this report are from global ocean wave model data sets and satellite radar altimeters. The main parameters of this study include; wind speed, significant wave height (swh) and wave period. These parameters will come from European Centre for Medium-range Weather Forecasting Wave Assimilation Model (ECMWF WAM) and satellite radar altimeter data. The area of study has been defined as 66^{o}N-10^{o}S, 110^{o}W-10^{o}E, which is the North Atlantic slightly extended south, to investigate teleconnections from the tropical Pacific which may influence wind and wave variability. The time period of this study is from September 1992 - July 2009 for the full ERA-Interim data and May 1995 – December 2008 for the extended satellite data. Direct comparisons of the model data and satellite data span from September 1992 – August 2002 and January 1993 – August 2002, respectively.

Global ocean wave models are driven by modelled and measured oceanic wind fields. Validated wave models can increase the available observations by interpretations and interpolations and allow evaluations of possible cause and effect of wind and wave variability (Woolf and Wolf, 2006). The wave models attempt to replicate the growth, decay and propagation of ocean waves based on input winds. The current state of the art of the science

of wave modelling can be found in Cavaleri *et al* (2007) and references therein. The wave model datasets used in this study are from the ECMWF Re-Analysis models (ERA-40 and ERA interim) (see http://www.ecmwf.int/research/era/do/get/index). The output from the wave model will be analysed to test whether it can replicate the seasonal and interannual variability of wind and wave data found from the satellite data. It should be noted that the Re-analysis models assimilate ERS-2, Jason-1 and Envisat wind and wave data and therefore this has to be accounted for when making comparisons. A second aim is to link anomalous values over an area with anomalous climate indices to explain the variance patterns.

The satellite radar altimeter is a nadir pointing radar that transmits pulses vertically downward and measures the time of travel, shape and power of the back-scattered signals. The satellites used in this study include the TOPEX, Jason-1, ERS-2 and Envisat, which have all been calibrated against buoy data (Cromwell and Gommenginger, 2009). The calibrated satellite data offer swh and the zero up-crossing wave period (T_z). In addition, the 10 day repeat cycle of TOPEX + Jason-1 will be compared to the 35 day repeat cycle of ERS-2 + Envisat.

Young (1999) calculated the variability of wind speed and swh globally, based on different satellite altimeter products available at the time. This data was used to improve the raw data of the satellite products and compare them. However, the use of GEOSAT, TOPEX and ERS-1 in the study only provides a relatively short period of data and do not show any change in the global wind and wave climate over the 10 years sampled by the various missions at that point in time. The time span of the data used in this study will allow comparisons to be made with the wind speeds from the modelled data and to increase the length of study, from Young's 1985 – 1995 period. Chen *et al* (2003) has studied the spatial variability of global

winds from 1993-1998 with TOPEX altimeter data, but focused mainly in the Southern and Indian Ocean. Additional wind studies have been completed using Synthetic Aperture Radars (SAR) (Young, 1999b) as they can directly measure wind direction as well as wind speed. However, few studies have recently looked at wind variability from model data, especially ERA-interim which has only become available recently. The North Atlantic is known to have a very variable wind climate. Average wind speeds range from approximately 15.1m/s to 7.9m/s in winter and summer, respectively (Young, 1999b). Wind variance is a very important influence for swh and wave period in the North Atlantic (Bauer and Weisse, 2000), due to atmospheric baroclinic instabilities, the passage of atmospheric fronts and location and intensity of storm tracks. Sterl and Caires (2005) have studied wind speed variability for each of the major basins using ERA-40 wind speeds.

The availability of climatologies of swh has lead to more studies of its variability. Cotton *et al* (1997) showed using altimeter data on a global scale, that in one hemisphere if the wave climate is calmer than usual during a particular year, the wave climate is rougher in the other hemisphere, perhaps due to a planetary atmospheric mode and the influence of seasons. Longer time scale variability is common in certain areas which are subject to large changing atmospheric modes. The atmospheric modes represent the changing pressure patterns which affect wind speed on a range of time and space scales. Cotton and Challenor (1999) found large levels of spatial variability within most oceanic basins, as some regions show a rise in swh whereas others show a fall. Sasaki and Hibiya (2007) have recently used the ERA-40 re-analysis wave data as well as TOPEX/Poseidon data to determine the interannual variability of swh during summertime in the western North Pacific. Most of the variability resulted from atmospheric forcing, as the first EOF was closely correlated with zonal wind anomalies within the NINO 3.4 region (**Figure. 2.4.**). This study also further evaluates the limitations of

ERA-40 data, which are useful when identifying the differences between ERA-40 and ERA-Interim products.

Wave model data have also been previously compared against in-situ and satellite data. Gulev *et al* (1998) compared datasets for the North Atlantic from 1979-1993. The in-situ observations were from mid latitudes and higher latitudes by Voluntary Observing Ships (VOS). The results showed that the WAM hindcast swh were overestimated by 0.1 to 0.3 m. Underestimations of the altimeter swh were also found by approximately 0.1-0.2m. However, data from VOS has to be used with caution. Wolf and Woolf (2006) have recently studied the North Atlantic wave field using a regional wave forecast model. They show influences from storm tracks to have a large effect of wave variability. Results from this study can be compared to data from the global wave models and to see if the same variability is present. Caires and Swail (2004) show trends of the changing wave climate in the North East Atlantic of approximately a 2.6cm/yr increase, whereas the mid-Atlantic shows a decrease of approximately 1.5cm/yr, during January, February and March in the time period of 1958-1997.

The variability of wave periods has only recently been studied using satellite altimeter data by Sykes (2005) in the North Atlantic for 11 years, 1993-2004. This included the parameters of: the mean wave period (T_m), peak wave period (T_p) and zero-upcrossing wave period (T_z) using altimeter data. Wave period climatologies have been studied by Young (1999) and Sterl and Caires (2005) who used the entire ERA-40 dataset. The longest waves are known to occur in the North Atlantic along the coasts of western Europe and are slightly shorter compared to those in the North West Pacific. The time period of this study, from 1992-2009

will allow use of the observations to test whether the wave period has become more or less variable in recent years.

It has been known for a while that the North Atlantic Oscillation (NAO) and other modes of atmospheric variability influence the wave field across the North Atlantic mainly in the winter months, except for a few regions (Woolf *et al*, 2003). The North Atlantic is one of the most variable oceans in the world. It is not influenced by swell from the southern hemisphere due to its narrow basin size, unlike the other major oceans such as the Indian Ocean and Pacific Ocean (Sterl and Caires, 2005). This dissertation will focus on the North Atlantic, as have most previous studies (Bacon and Carter, 1991; Günther *et al*, 1998; Woolf *et al* 2002; Sykes 2005), and will seek to validate whether wave models can correctly reproduce the observed wave field dependence on the state of the Northern Atlantic Oscillation (NAO), East Atlantic Pattern (EAP) and possible teleconnections from El Niño Southern Oscillation (ENSO) and any other possible modes of atmospheric variability.

Previous variability and climatologies of the entire ERA-40 dataset of swh, mean wave period (mwp) and wind speed has been studies by Sterl and Caires (2005) using the C-ERA-40 dataset - a corrected version of the ERA-40 swh and mwp produced with KNMI (Koninklijk Nederlands Meteorologisch Instituut) to give the Web-based KNMI/ERA-40 wave atlas (http://www.knmi.nl/onderzk/oceano/waves/era40/license.cgi), which reduced the root mean square (RMS) difference by validation from buoy data and satellite altimeter. They also removed some of the time inhomogeneities, which gave higher swh and mwp results, caused by the faulty ERS-1 which was assimilated.

2.1. Modes of atmospheric variability

The state of the atmosphere greatly affects wave parameters because winds generate the waves. The changing pressure fields and temperature of the atmosphere affect the speed and direction of the wind. The directions of storm tracks are also influenced by the atmosphere and ocean. The atmospheric modes that will be investigated in this study are listed below:

2.1.1. North Atlantic Oscillation

The NAO relates to a distribution of atmospheric mass between the Icelandic low pressure centre and the Azores high pressure centre, throughout the year, which oscillates between two extreme phases given by the pressure gradient (**Figure. 2.1.**). This produces large changes in the mean wind speed and wind direction over the Atlantic, as well as the heat and moisture transport between the Atlantic and the neighbouring continents. NAO also influences the intensity and number of storms, their paths, and their weather, which can all affect wave parameters (Wallace and Gutzler, 1981; Hurrell and Deser, 2009). The positive phase of the NAO is associated with warmer and wetter conditions in Northern Europe and colder, drier weather conditions in South Europe during the winter months (Jones *et al*, 2003). As well as, the positive phase corresponds to stronger westerly winds across the Northern Atlantic (Hurrell and Van Loon, 1997; Wolf and Woolf, 2006). The negative phase causes the opposite weather patterns (**Figure. 2.1**). The NAO is variable on a range of space and time scales (Hurrell, 1995; Marshall *et al*, 2001; Wu and Liu, 2005). This variability can be seen in the position of the storm tracks across the North Atlantic, which has a great affect on wave parameters (Chang *et al*, 2002; Dupuis *et al*, 2006).

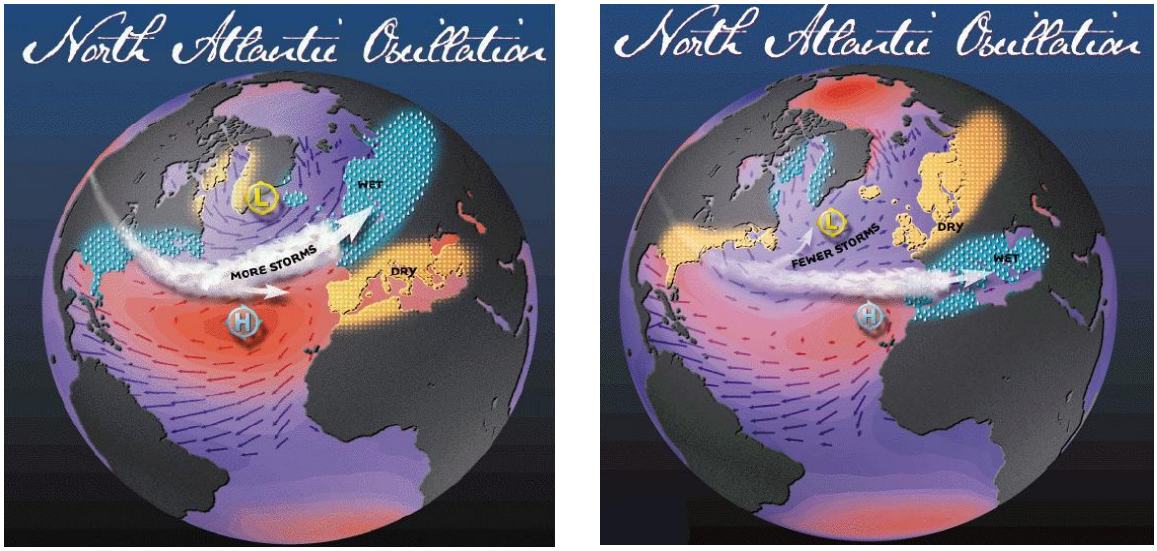

Figure. 2.1. NAO and its affect on climate parameters. left, NAO positive. right, NAO negative. Images from Visbeck [http://www.ldeo.columbia.edu/NAO].

2.1.2. East Atlantic Pattern

The EAP is the second most prominent mode of low-frequency variability over the North Atlantic, and appears as a major mode of variability throughout the year. The EAP is structurally similar to the NAO, and consists of a north-south dipole of anomaly centres spanning the North Atlantic from east to west (Josey and Marsh, 2005) (**Figure. 2.2.**). This arises due to changing sea level pressure which affects other surface parameters (Barnston and Livezey, 1987).

The positive phase is associated with above average surface temperatures in Northern Europe for all months and above average precipitation over both northern Europe and Scandinavia. In addition, it is characterized by a strong negative pressure anomaly in the NE Atlantic, which moves to the centre of the basin from December to March (Lionello and Galati, 2008). The EAP shows very strong multi-decadal variability.

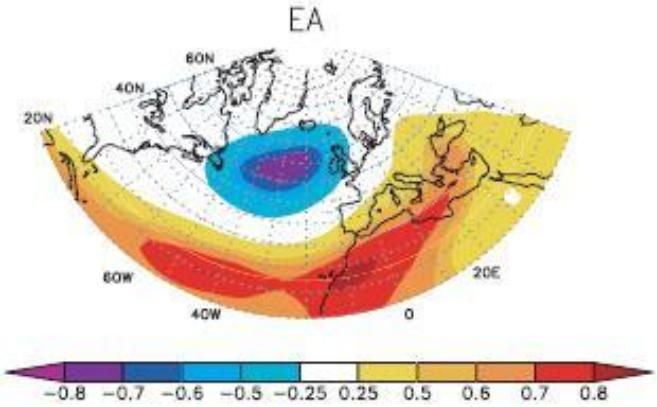

Figure. 2.2. Temporal correlation between the monthly standardized height anomalies at each point and the monthly EAP for December-February 1960-2000**.** Trigo *et al* (2008).

2.1.3. El Niño Southern Oscillation

The ENSO is the dominant mode of variability across the tropical Pacific and shows large variability interannually. It is caused by the change in wind speeds across the basin resulting from shifts in the movement of different atmospheric circulation patterns and is most dominant in the winter months (Wyrtki, 1975) (**Figure. 2.3.**). Its variability can affect parameters globally by means of atmospheric processes, usually on the order of a few months and oceanic processes which can take years to decades to affect other basins (Burgers and Stephenson, 1998; Alexander *et al*, 2002; Wu and Hsieh, 2004; Taguchi and Hartmann, 2005; Liu and Alexander, 2007). These are known as teleconnections.

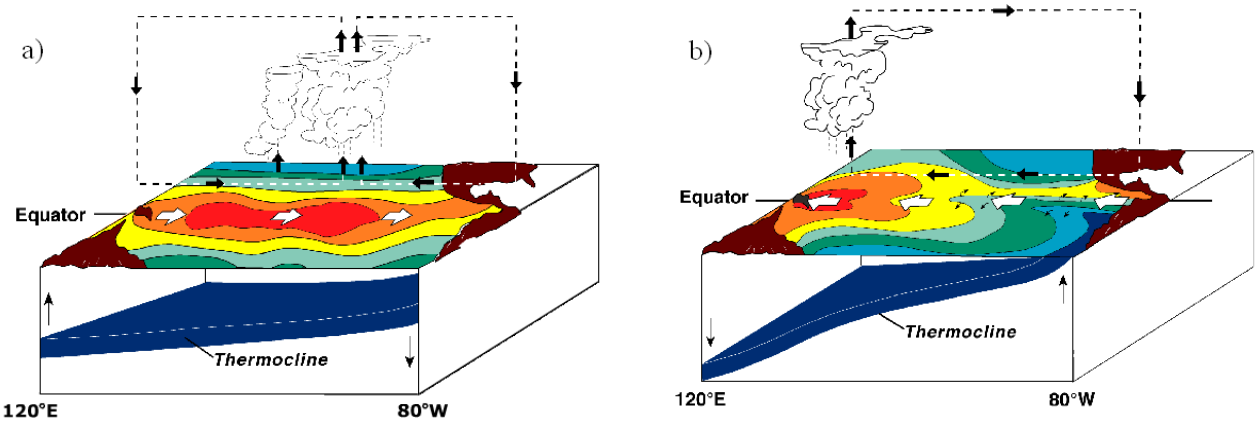

Figure. 2.3. A figure showing the atmospheric circulation and tilt of the thermocline during (left) El Niño and (right) La Niña. Tropical Atmosphere Ocean project (2000).

The Pacific region is commonly broken down into smaller areas to study regional climate. (**Figure. 2.4.**) These areas are often used for teleconnection studies. Anomalous wind speeds in the tropical Pacific can results in anomalous wind speeds in the North Atlantic by means of the atmospheric bridge. Energy and wave propagation transport signals as the atmosphere acts as a 'bridge' between basins. An initial change in the tropical Pacific can affect the regular Hadley cell circulation – the zonal atmospheric cell located approximately 0-30°N and 0-30°S. The anomalous signal can then be transported to the tropical Atlantic by atmospheric planetary waves and eddy-mean flow interactions and affect surface parameters. The anomalous results can be present months after the El Niño event due to the slow feedback time of the ocean parameters from the atmosphere, such as its effects on sea surface temperature and evaporation which affect wind speed.

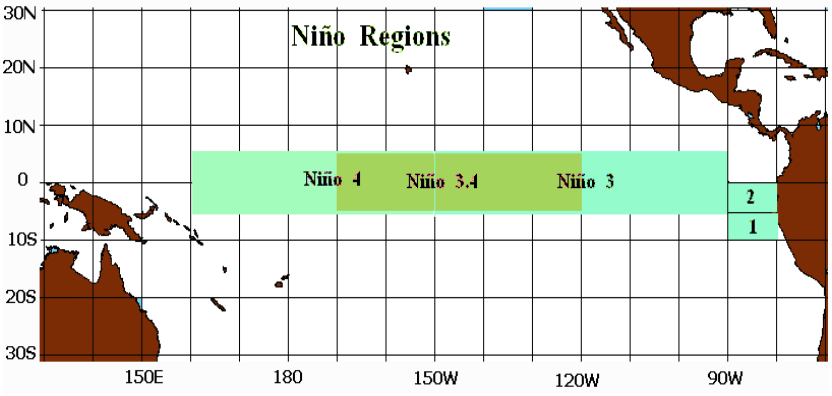

Figure. 2.4. A map of the NINO regions which are most commonly analysed. Gold Gate Weather Services. (2000).

3. Data and Methods

3.1. Global ocean wave models

The wave model data is provided from ECMWF WAM. The WAM model output is the two-dimensional wave energy spectrum $F(f,\theta)$ where f is the frequency and θ is the direction, obtained at each grid point by integrating the wave energy balance equation (Komen *et al*,

1994; Semedo *et al*, 2009). From these spectra several derived integrated wave parameters can be obtained. This provides the parameters of significant wave height (swh) and mean wave period (mwp); this is based on the −1 spectral moment, m_{-1}/m_0 (Caries *et al*, 2005). This is also known as the energy period (T_e) (Mackay *et al*, 2008) (**Appendix. 1.**). The atmospheric model provides u wind velocity at 10m height and v wind velocity at 10m. These were converted into wind speeds by squaring both components and taking the square route of their sum. The two model dataset which I will be using are ERA-40 and ERA-Interim. ERA-40 is a global analysis which describes the state of the atmosphere and ocean-wave conditions from mid-1957 to mid-2002, 45 years worth of data. ERA-Interim as the name suggests is an interim re-analysis, for the period 1989-present, in preparation for the next generation re-analysis to replace ERA-40. I downloaded ERA-40 and ERA-Interim datasets of daily files at 00:00 [data from: http://data.ecmwf.int/data/] on the 1st October 2009. The area of study has been defined as 66°N-10°S, 110°W-10°E, which is the North Atlantic slightly extended south. The time period of this study is 1992-2009. The ERA-40 data used spans from September 1992 – August 2002 whereas, the ERA-Interim data used is from September 1992 – July 2009.

3.1.1. ERA-40

ERA-40 is a second generation re-analysis and the first re-analysis to use an ocean-wave model coupled with an atmospheric model. The data is compiled using ECMWF's Integrated Forecasting System (IFS) (Simmons and Hollingsworth, 2002) with an updated 3D variational data assimilation (Andersson *et al*, 1998; Caires and Sterl, 2003). The model switched to 4D variational data assimilation in November 1997 (Rabier *et al*. 2000). The data assimilated into the model has changed over time with an increase in satellite input onwards from 1970s, a recent increase in airborne observations and ocean buoys (**Figure. 3.3.**).. In the later years it assimilated scatterometer and Special Sensor Microwave Imager (SSM/I) data.

It assimilates data from ERS-1 after December 1991 and ERS-2 after June 1996 of ocean wave heights and surface wind speeds (Sasaki and Hibiya, 2007). In addition, a decreasing

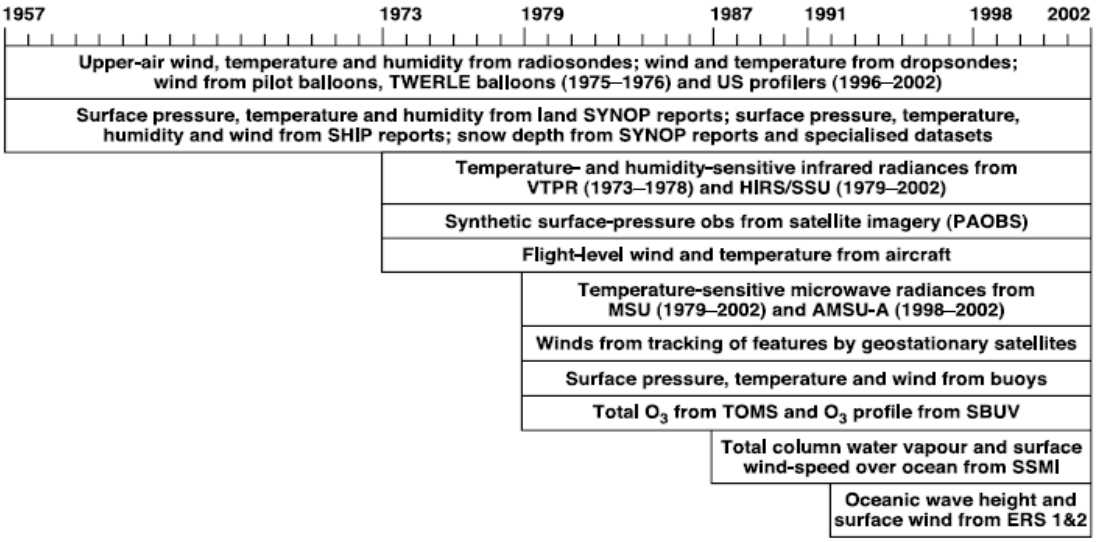

Figure. 3.3. Chronology of types of observation assimilated in ERA-40. See Uppala *et al* (2005) for acronyms

number of radiosonde data used was from 1980s onwards (Uppala *et al*, 2005). The freely available ERA-40 wave re-analysis covers the globe with a resolution of 2.5^{o} x 2.5^{o} latitude and longitude. It covers the time period from September 1957 – August 2002 at 6 hour intervals. Due to the grid spacing of the data, the North Atlantic extends from 67.5°N-10°S, 110^{o}W-10^{o}E.

The WAM (Komen *et al*, 1994) is forced by hourly winds from the latest 6-hour forecast instead of by the analyzed winds (Janssen *et al*, 2002). The ERA-40 output comprises the full directional wave spectrum. The swh is computed as 4 times the square root of the 0-order spectral moment (Uppala *et al*, 2005) (**Appendix. 1.**). It should be noted that data of swh and mwp have inhomogeneities from Dec 1991 – May 1993 due to the assimilation of faulty ERS-1 Fast Delivery Product (Bauer and Staabs, 1998).

3.1.2. ERA-Interim

ERA-Interim is the most recent re-analysis provided by ECMWF. It is based on a slightly different IFS to that of ERA-40. It contains some improvements on ERA-40 such as the complete use of four-dimensional variational data assimilation (Berrisford *et al*, 2009). ERA-Interim is the first re-analysis using adaptive and fully automated bias corrections of satellite radiance observations (Dee and Uppala, 2008). It uses the latest cycle of an updated atmospheric model (IFS Cy31r1/2) which includes increased pressure levels and additional cloud parameters, taking an advantage of improved model physics (Simmons *et al*, 2007) (for more information of the Integrated Forecast System see http://www.ecmwf.int/research/ifsdocs/index.html). ERA-Interim has built on the satellite data assimilation in ERA-40 and includes recent satellite data such as altimeter wave heights; a new ERS altimeter wave height dataset has been acquired, providing data of more uniform quality than the fast delivery dataset used from August 1991 onward in ERA-40. ERS-2 was assimilated from May 1995 – July 2003 and there are now ongoing assimilations from Envisat and Jason-1 which started in July 2003 and October 2003, respectively. The model also assimilates new wind observations from Meteosat reprocessed winds. Internal validation of the ocean wave height analysis produced with ERA-Interim also indicates a higher degree of homogeneity. An updated version of WAM includes a revised formulation of ocean wave dissipation which has reduced the RMS error in T_z against buoy data and shows they are stable and much smaller than in ERA-40 (Bidlot *et al*, 2007). Also there is reduced 10 m wind speed bias over extratropical ocean areas in the northern hemisphere (Uppala *et al*, 2008). For the complete ECMWF users (not the free online version) ERA-Interim is able to resolve 30 wave frequencies and 24 wave directions which are higher than the complete ERA-40 resolution; 25 frequencies and 12 directions.

The data was downloaded for the whole time period of September 1992 – July 2009 of daily files with a resolution of 1.5^{o} x 1.5^{o} latitude and longitude. Due to the grid spacing the North Atlantic section is from 66°N-10°S and extends to 111°W and 10.5°E, instead of 110°W, 10°E.

3.2. Satellite radar altimeters

I will be using 4 satellite radar altimeter datasets, including dual frequency altimeters on TOPEX (TOPographic EXperiment), Jason-1, Envisat (Environmental satellite) and the single frequency altimeter on ERS-2 (European Remote Sensing satellite). TOPEX and Jason-1 use the C band (5.3 GHz) and K_u band (13.6 GHz) to measure sea surface height, whereas Envisat uses the K_u and S band (3.2 GHz). The lower frequency band is used to account and correct for ionospheric delays in K_u-band range measurements (Robinson, 2004). ERS-2 samples in the K_u band only. Dual frequencies are more accurate than mono frequency altimeters (Robinson, 2004). These altimeters sample along track approximately every second. The satellites offer different spatial resolution to the model data. ERS-2 and Envisat have a 35 day repeat cycle and offer higher across track spatial resolution of the sea surface in comparison to TOPEX and Jason-1 which have a 10 day repeat cycle and offer a lower across track spatial resolution. The different satellites therefore trade higher spatial resolution for a longer re-visit time. ERS-2 and Envisat give three times the spatial resolution compared to TOPEX and Jason-1 but only offer one measurement per month. Whereas, TOPEX and Jason-1 give three measurements per month and are likely to pick up more high frequency variability. I will examine which type of space sampling gives the more accurate result. The along track results will be gridded in using a 2D Gaussian function (Cromwell and Gommenginger, 2009) to produce monthly global averages. The altimeter results are calibrated with buoy data used with a maximum separation in time of 30 minutes and spatial

separation of up to 100km using orthogonal distance regression (Cheng and Van Ness, 1999). I will then extract data for the area of study (66°N-10°S, 110°W-10°E).

The altimeter works by sending out a nadir directed pulse of microwave radiation continuously along its track which reflects back from the sea surface as backscattered return. The return can then be used to obtain geophysical properties of the ocean (Fu and Cazenave, 2001). The backscattered power (σ^o) is given by the amplitude of the return pulse which is used to estimate wind speed. As wind speed increases the surface becomes rougher and larger waves are produced. This results in more of the signal being reflected away from the altimeter and lower amplitude return (**Figure. 3.1.**)

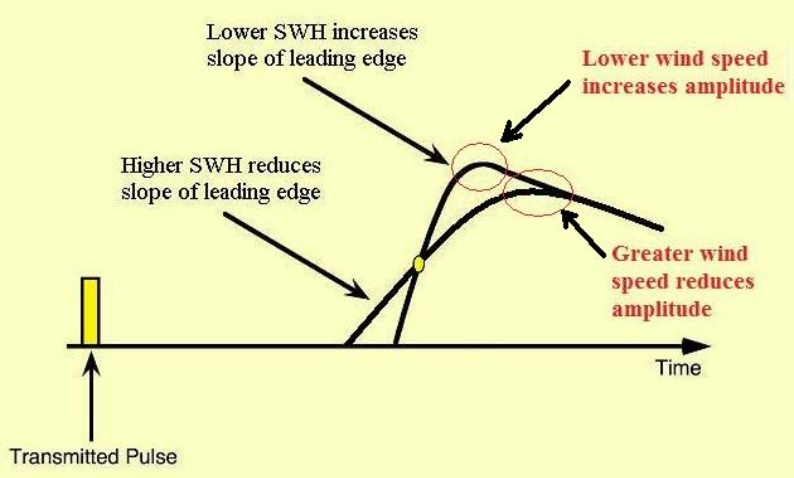

Figure. 3.1. Schematic of the satellite radar altimeter and what geophysical properties can be obtained from it. (Adapted from Sykes, 2005)

The slope of the leading edge of the return pulse changes as the pulse is reflected by an uneven surface and decreases with increasing swh (**Figure. 3.1.**). The stretching effect of the signal is caused by the time delay of returns from the wave crest first and the wave trough later. swh is defined as four times the square root of the variance of the sea surface elevation (**Appendix. 1.**).

Wave period can be calculated indirectly as a model based on an algorithm from swh and σ^0 (Hwang *et al*, 1998; Davis *et al*, 1998; Gommenginger *et al*, 2003; Quilfen *et al*, 2004; Mackay *et al*, 2008). The definition of wave period depends on the way it is measured. T_z is now mostly studied with altimeters and can be defined as the mean of the time interval between 2 successive up-crossings of the mean water level (Tucker and Pitt, 2001), where T_z is defined as $\sqrt{m_o / m_2}$ (**Appendix. 1.**) Gommenginger *et al* (2003) developed a simple empirical model to retrieve wave period using the K_u-band with RMS difference from buoys of 0.8s. They relate σ^0 to the inverse of the mean square slope of long ocean waves (Barrick, 1974) and use buoy data for validation. The model was found to work best for wind driven waves. Quilfen *et al* (2004) proposed an improved model taking into account the K_u band, swh, σ^0 and sea state maturity; this reduced the RMS difference to 0.69s for T_z with buoy data. The model is valid for σ^0 up to 16 dB; however, it is limited measuring high wave period waves. Mackay *et al* (2008) present the most recent and accurate model for calculating wave period from altimeters. They create a parametric model with different equations for σ^0 below 13 dB and greater than 13 dB. This reduces the RMS difference of the Quilfen *et al* (2004) model by 15% (**Figure. 3.2.**). Mackay *et al* (2008) use a large collocated data set of altimeter and buoy measurements, to validate their study, similar to Caires *et al* (2005).

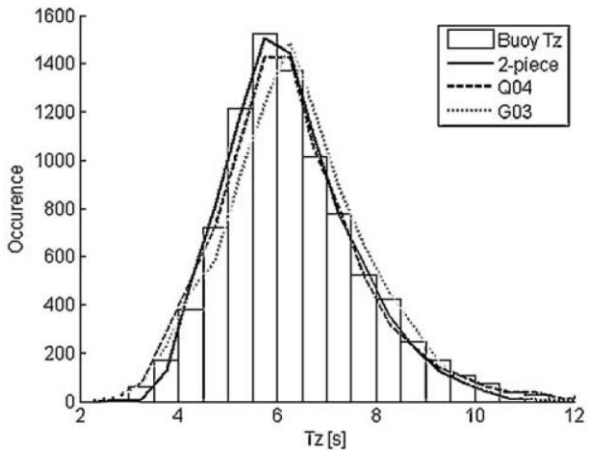

Figure. 3.2. Histogram of buoy and altimeter T_z. G03 is the Gommenginger *et al* (2003) model, Q04 is the Quilfen *et al* (2004) model and the 2-peice is the Mackay *et al* (2008) model. (data is σ^0 < 16 dB with comparison with Q04). Mackay *et al* (2008).

3.3. Climatologies

Monthly climatologies were produced by firstly creating monthly files from the daily files for the model data and taking the mean of those months. Secondly, from the mean value for a particular month I subtracted the long term mean for that month, in the time series for all the parameters in both the altimeter data and ERA model data, to remove the seasonal cycle and give monthly anomalies; ERA-40 September 1992 – August 2002 and ERA-Interim September 1992 – July 2009. I also created these for the ERA-Interim dataset from Sep 1992 – August 2002 for a direct comparison between the two model datasets. I calculated the standard deviations (std) for the monthly climatologies in the full ERA-Interim dataset as a simple measure of the interannual variability.

I produced monthly climatologies and anomalies for swh and T_z from TOPEX for the time period January 1993 – August 2002 as the closest direct comparison to the model data. The entire TOPEX data spans from January 1993 – October 2005. I also produced longer satellite time series datasets from May 1995 – December 2008. Firstly, TOPEX (May 1995 – December 2002) + Jason-1 (January 2003 – December 2008) (tx-j1 hereafter). For reference the Jason-1 time period is February 2002 – December 2009 (although the data has only been calibrated with buoy data up to December 2008). To compare this with altimeters with a longer re-visit time and higher spatial resolution I used ERS-2 (May 1995 – December 2002) + Envisat (January 2003 – December 2008) (e2-n1 hereafter). ERS-2 data starts in May 1995, so the results do not extend further beyond this and extends to September 2003. The full Envisat data is available from October 2002 to September 2009. The ERS-2 T_z was shown to give negative values in the Great Lakes therefore there were replaces with NaN's similar to

the land. The results can also loosely be related to the full ERA-Interim dataset and show a recent change in the wave climate from the earlier TOPEX data.

The difference in resolution between the datasets is ignored and the location of values is of more importance. This will allow for an easier visual comparison between the model and satellite datasets.

3.4. Empirical Orthogonal Function analysis

EOFs provide a compact description of the spatial temporal variability of data series in terms of orthogonal functions (Emery and Thomson, 2001). The low order EOFs (the first few orthogonal functions) can sometimes be interpreted as natural modes of variation of the observed system, such as atmospheric patterns/oscillations (Storch and Francis, 2001). The EOFs can be mapped as spatial patterns of variability and the associated time series – referred to as principal components (PC) - each of which describes the time evolution of the corresponding spatial structure (Preisendorfer, 1988). One should be aware that the EOF analysis is a mathematical construct of mutually orthogonal eigen-vectors. There is no guarantee that they represent a physical or dynamic mode in the climate system (Dommenget and Latif, 2002).

The first 4 EOFs will be studied as they will allow for a visual comparison between the datasets. The first 4 EOFs are likely to show the atmospheric modes (section **2.1**) and are expected to explain a large percentage of the variance.

3.5. Climate indices

Climate indices will be correlated against the PCs from the EOFs with time to observe if the atmospheric modes can explain the observed variability in the wind and wave field. The atmospheric modes of the NAO and EAP will be correlated against the first and second EOF as they are likely to explain the dominant and secondary mode of variability. It was noticed than the first and second EOFs of wave period showed poor correlation with either the NAO or EAP, however the spatial pattern of the third EOF looked similar to the NAO so I included this in the correlation. If the correlation is statistically significant at the 95% confidence interval this will be displayed on the plot.

In addition, monthly anomaly plots of a particular parameter will be regressed against a climatic index anomaly in space to observe how the correlation varies in the extended North Atlantic basin of 66°N-10°S, 110°W-10°E.

3.5.1. NAO and EAP

The Monthly indices of the NAO and EAP were downloaded from the National Oceanographic and Atmospheric Administration Climate Prediction Centre (NOAA CPC) [ftp://ftp.cpc.ncep.noaa.gov/wd52dg/data/indices/tele_index.nh]. The NAO indices are derived from the rotated principal component analysis (RPCA) used by Barnston and Livezey (1987). This method isolates the primary teleconnection patterns for all months and allows a time series to be constructed. The RPCA is applied to monthly mean standardized 500-mb height anomalies obtained from NOAA's Climate Data Assimilation System (CDAS) in the analysis region 20°N-90°N between January 1950 and December 2000. The anomalies are standardized by the 1950-2000 base period monthly means and standard deviations, which uses a three month window. The 12 sets of rotated modes - one for each mode - revealed ten dominant teleconnection patterns. The primary mode represents the NAO and the secondary mode represents the EAP, these will be used in this study.

3.5.2. Multivariate ENSO index

The Multivariate ENSO index (MEI) created by Wolter and Timlin (1993) uses six main observed variables across the tropical Pacific: sea level pressure, zonal and meridional components of surface wind, sea surface temperature, surface air temperature and total cloudiness fraction of the sky [http://www.esrl.noaa.gov/psd//people/klaus.wolter/MEI/table.html]. Each field is set into clusters (Wolter, 1987) and the total variance of each field is normalised. The first PC on the co-variance matrix of all six fields combined creates the MEI which is given as twelve sliding bi-monthly values.

3.6. Spatial correlations

Each monthly climate index anomaly was regressed to the monthly model parameter anomaly at each grid cell of my North Atlantic basin for the whole time series of ERA-Interim (Woolf *et al*, 2002). The MEI was lagged up to 3.5 years – approximately half the period of ENSO events - to observe the changing teleconnection patterns into the North Atlantic. In addition, I did this with the most accurate satellite data for swh and T_z to complement the model data.

I carry out cross-correlations on time series of climate index anomalies and parameter anomalies, where the error estimates for the correlations are at the 95% confidence level, where the null hypothesis assumes that there is no correlation between each pair of time series. The effective degrees of freedom is calculated for each pair of time series, where the coherence and autocorrelation of the data is taken into account when estimating the degrees of freedom (Emery and Thomson, 2001).

4. Results and discussion

4.1. Climatologies, monthly anomalies and standard deviations

4.1.1. ERA wind speed

The climatology of wind speed from ERA-40 is shown in (**ERA40_wind_clim.mov**). The wind speed shows a pattern of zonal bands which alternate from high to low. The peak wind speeds can be found north of 35°N in January and February with values of 12-13 m/s and reach a low in August in the 30°N band at 3 m/s. The band of high wind speed at 50-60°N moves slightly north eastward in February. The summer months show alternating zonal bands of low and high values.

The anomalous results in **ERA40_wind_anom.mov** show wind speed is the most spatial variable parameter in the North Atlantic. The anomalous values are present all year round and all in the basin of the North Atlantic. The winter months show the largest change in wind speed compared to the summer months. The large anomalous areas in particular months are closely related to the anomalous swh months (**ERA40_swh_anom.mov**) but the links with mwp are not obvious (**ERA40_mwp_anom.mov**).

A slightly higher wind speed in ERA-Interim for the time period of September 1992 – August 2002 can be observed in the climatology of September at 55°N, 40°W but only by approximately 0.1-0.2 m/s (**ERAint_wind_clim_short.mov**). The difference in wind speed between the two models is largest in April by ~0.2 m/s, north of 40°N.

There are only minor differences between the two models in terms of their respective monthly anomalies (**ERAint_wind_anom_short.mov**). In September 1992 ERA-Interim gives slightly lower values of wind speed in the central North Atlantic and higher values of wind speed across 10°N. In other months the North Atlantic wind speeds are very similar

however, they differ between 10°N-10°S the most as ERA-Interim gives slightly larger values of 0.5-1 m/s in February 1994.

The full ERA-Interim climatology (**ERAint_wind_clim.mov**) shows a wind speed maximum in December at 50°N, 40°W and February of 12 m/s which is slightly smaller than the shorter ERA-Interim climatology. This suggests there has been a slight decrease in winter wind speed during the 2000s in comparison to the 1990s. The summer months show similar wind speeds for both time series.

The monthly anomalies of ERA-Interim wind speed after August 2002 show December 2002 has zonal bands of higher than normal wind speed at 50°N, lower at 35°N and higher again at 20°N (**ERAint_wind_anom.mov**). A large change in wind speed is obvious in March 2005 as some areas show increases of 2.5m whereas others show a decrease of 2.5m. February 2009 shows in increase in wind speed in the north east of up to 2.5 m/s and a decrease of 1.5 m/s in the south

The std of the monthly climatologies from the full ERA-Interim dataset is shown in **ERAint_wind_std.mov**. February gives the largest variation north of 40°N and east of 40°W at > 1.5 m/s. July shows the lowest std value throughout the extended North Atlantic with values as low as 0.2 m/s whereas the north east region in the winter months shows the largest variability. The maximum std in ERA-Interim is similar to the maximum std obtained by Sterl and Caires (2005) for the ERA-40 dataset from 1971-2000. However, the differences occur in the location of maximum std. February shows less of an increase north of the British Isles and more south west to 50°N, 20°W, showing a change in the location the maximum variability in February.

The maximum wind speeds occur in the winter months in the northern region as the prevailing westerlies are at their strongest (Chen *et al*, 2003). The trade winds in the south

part of the basin and near the equator are low all year round and therefore wind speed does not deviate greatly from its low speed (Chen *et al*, 2002). The anomalous months arise due to changes in atmospheric modes, which are studied with EOFs (**4.2.1.**). The accuracy of the wind speed has a large influence on how accurate the wave field is. There are strong links of anomalous wind speed to anomalous swh but not so for anomalous mwp.

The climatologies from ERA-40 and ERA-Interim show the data are very similar except for minor increases in maximum wind speed in ERA-Interim. The increase in resolution of ERA-Interim may be allowing for better resolution of the most extreme and intense storm events and explaining the larger values (Wolf and Woolf, 2006). However, the maximum wind speeds of ERA-Interim are still lower than those obtained from satellite data. Sterl *et al* (1998) found that ERA-40 winds are too low in areas of higher wind speeds by forcing the WAM with the ERA-40 winds and comparing against altimeter swh observations. The wind speeds of ERA-40 are also underestimated in comparison to other re-analysis winds; National Centres for Environmental Protection/National Centre for Atmospheric Research (NCEP/NCAR) (Wolf and Woolf, 2006) and ERA-15 (Sterl *et al*, 1998; Uppala, 2005). In January ERA-Interim gives a maximum of 13 m/s where as Young (1999b) obtained 15.1 m/s and ERA-Interim also gives slightly lower wind speeds of 6.5 m/s compared to the minimum wind speeds obtained by Young (1999b) of 7.9 m/s, albeit a slightly different time period.

4.1.2. ERA swh

The animation of ERA-40 swh climatology from September 1992 – August 2002 is shown in **ERA_40_swh_clim.mov**. The northern region of the North Atlantic above 30°N shows the most dynamic change throughout the year. The area south of 30°N has little variability, approximately 1-2m throughout the year. The swh is greatest in the winter months and the maximum swh occurs in January as values reach 5m. In February the area of greatest swh is

shifted north eastwards to 58°N, 20°W. The lowest swh occurs in August as it ranges between 1.5m and 2.5m throughout the North Atlantic. The Mediterranean and North Sea show very low values and do not show as much variability compared to the surrounding offshore areas. The swh in the Mediterranean reaches a maximum of approximately 1.2m in December whereas, a maximum of 3m in February for the North Sea.

The anomalous months are shown in **ERA_40_swh_anom.mov**. January 1993 shows a large decrease in swh of -1.5m around the British Isles, whereas in February 1993 there is an anomalously high area at 48°N, 16°W. The summer months show negligible changes. In December 1993 a high appears at 38°N, 22°W of 1m as well as a low around the south west of the British Isles of -1m. January 1996 also shows large areas of high swh along with areas of low swh similar to December 1993. January 1997 shows an increase in swh to the west of Ireland. February 1997 shows a large decrease to the south west of Ireland and March shows lower swh in the northern region.

The ERA-Interim swh animation on the same time scale as the ERA-40 data is shown in **ERAint_swh_clim_short.mov**. The September climatology of the ERA-Interim dataset gives slightly higher values of approximately 0.1-0.2m in the northern region of the North Atlantic compared to ERA-40. January shows the largest difference in maximum swh between the two model datasets. The values are approximately 0.3m higher and the location extends further north eastwards to 60°N, 12°W in ERA-Interim. In February the high values extends slightly more south westwards. The swh lows are of similar values and at similar locations in both model datasets. Lower values are also present at the coastal locations in comparison to ERA-40; this can be seen clearly off the east coast of North America in the winter months.

The slight difference in anomalous results can be seen in February 1993 (**ERAint_swh_anom_short.mov**). The area of highest swh is much larger in ERA-Interim.

March 1993 shows greater values of swh in ERA-Interim. However, some months show more of decrease of swh in ERA-Interim such as March 1994 around Ireland.

The swh climatology for the whole ERA-Interim data set September 1992 – July 2009 can be found in **ERAint_swh_clim.mov**. The maximum swh area in December and January slightly decreases in size for the extended time series in comparison to the September 1992 – August 2002. The maximum swh in February decreases by 0.3m showing a calming of the North Atlantic winter months in recent years whereas the summer months are very similar.

Monthly anomalies of swh from ERA-Interim can be found in **ERAint_swh_anom.mov**. The anomalous months up to August 2002 are similar to those obtained in the shorter time series but are calculated from a different climatology. I will therefore only comment on anomalous months after this date. November 2002 shows a large decrease in swh of up to -1.5m at 50°N, 25°W. In February 2004 there is an increase in swh of over 1m in the central northern region. The swh climate is highly variable in March 2005 as a dividing line emerges from the tip of Greenland to North West Spain. The winter of 2009 only shows slight changes from the climatology in swh as January is 0.8m lower in the north east region and February is higher in the same region by approximately 1m.

The std of the ERA-Interim swh can be found in **ERAint_swh_std.mov**. The animation shows standard deviation is low from May to September, as the std does not surpass 0.3m, especially in the tropical zone as the winds are not variable (Baxevani *et al*, 2007). In January high variability can be seen on the edge of the Hebridean shelf just north west of the British Isles (Woolf *et al*, 2003). February has the greatest variability as std reaches 1m, 20% of the mean. South of 30°N shows little variability in all months as std does not become larger than 0.3m. The results are similar to Wolf *et al* (2002) who studied the time period of August 1991 – February 2000, however, the maximum variability in February is slightly more southwards.

4.1.3. Altimeter swh

The climatology of swh calculated from TOPEX for the time period of January 1993 – August 2002 is shown in **tx_swh_clim_short.mov**. The swh is greatest in January as it reaches almost 5.8m, larger than the model dataset by ~0.6m. The TOPEX data also gives larger maximum swh results in February by ~0.6m. The swh is smallest in August with values of 2m across the entire North Atlantic, similar to the model data. The Mediterranean region in the satellite data shows a maximum of 2.8m, slightly larger than ERA-Interim and ERA-40 approximately 2.5m and 2m, respectively in the winter months. The monthly anomalies show some amount of trackiness in the data as the different altimeter passes produce slightly different results within a month (**tx_swh_anom_short.mov**). This becomes even clearer in comparison to the model data (**ERAint_swh_anom_short.mov**).

The longer satellite time series data from TOPEX (May 1995 – December 2002) + Jason-1 (January 2003 – December 2008) swh climatology is given in **tx_j1_swh_clim.mov**. The maximum swh slightly decreases in February in comparison to the earlier TOPEX dataset, which furthers the slight decrease in swh in winter months in recent years by ~0.2m. The monthly anomalies from the dataset are shown in **tx_j1_swh_anom.mov**.

The swh climatology for the satellite dataset of ERS-2 (May 1995 – December 2002) + Envisat (January 2003 – December 2008) is given in **e2_n1_swh_clim.mov** and **e2_n1_swh_anom.mov** shows the monthly anomalies. The results between the different satellite climatologies show tx-j1 give slightly larger maximum swh values of up to 0.1m in September in comparison to e2-n1 north of 45°N and east of 50°W. e2-n1 gives slightly larger swh in December north of the British Isles, whereas tx-j1 gives slightly larger values in the northern region in January and February, however swh in April – August are similar. The

differences in anomalous months are likely to arise from the slightly different monthly climatologies.

The winter months show the largest swh and most variability as the NAO can be at its most extreme phase, throughout the year. The resultant redistribution of pressure masses increase wind speed in the North Atlantic. An increase in zonal wind during the NAO positive state increases the amount of time in which the waves are built up and also causes an increase in storminess (Wolf and Woolf, 2006). The magnitude of swh is also influenced by swell components which arise from the frequency and intensity of distant storms (Trenberth *et al*, 2007; Trigo *et al*, 2008). swh is low around the equator due to the minimum wind values in the trade wind belts which cause the waves to be dispersive (Young, 1999b). The location of the anomalous areas can be explained to some extent by the behaviour of the NAO throughout the 1990s (Woolf *et al*, 2002) as the NAO switched from positive to a negative state around winter 1996. The EAP is also known to have a large affect on the wave climate in more recent years. Sykes (2005) found towards the end of his time series of 1992-2004 the EAP had more of an influence whereas the NAO has less of an influence on the winter months. The swh anomalies are closely related to the wind speed anomalies, which shows the strong relation that wind speed has in driving the waves. In the north west and northern North Atlantic the wind speed seems to play a more significant role in determining the wave height than does the fetch (Young, 1999). However, this is not always valid especially when the wind speed anomalies are not significant.

The larger values in ERA-Interim compared to ERA-40 are likely to be more accurate as the satellite data shows larger values for the maximum swh. ERA-40 and ERA-Interim assimilate altimeter wave height therefore do not allow for a direct comparison to the altimeter data (Greenslade and Young, 2004; Greenslade and Young, 2005). However, I can compare how

the re-analysis model maps the data homogenously in time and space in comparison to the actual satellite data. Other studies show that the maximum model swh is underestimated. Sykes (2005) showed that swh climatology of 1993-2004 in the winter reached up to 6m using altimeter data. In addition, Young (1999b) showed the northern region of the North Atlantic to have a swh up to 6m in the winter months from the climatology of 1991-1999 using altimeter data. The low ERA-40 wind speeds in the Mediterranean are likely to have caused the reduced ERA-40 swh in comparison to altimeter data (Ponce de Leon, 2008).

The model climatology results are similar to other studies of ERA-40 swh on an extended time series from 1971-2000 (Sterl and Caires, 2005) showing the swh from September 1992 – August 2002 has not deviated much from this. However, Sterl and Caires (2005) noticed that the results were lower than altimeter results especially in the winter months. An investigation into the ERA-40 swh data showed that a faulty fast deliver product (FDP) from ERS-1 wave height data, which is assimilated into the model caused swh below 3m to be overestimated and those above 3m to be underestimated. This was slightly improved after June 1996 as the FDP from the ERS-2 assimilation gave better swh results especially in the tropics (Sterl and Caries, 2005). This led to Sterl and Caires (2005) creating the C-ERA-40 dataset from 1970-2000.

4.1.4. ERA mwp

The largest change in mwp can be observed in the North East Atlantic throughout the year which ranges from approximately 11s in January to 7s in July (**ERA40_mwp_clim.mov**). Most variability occurs north of 20°N and there is a clear cut off of high mwp values west of Barbados at 15°N, 60°W. mwp reaches its maximum in the north east region in January with a build up and wind down 3 months either side. mwp is higher in the eastern North Atlantic compared to the western North Atlantic in all months. mwp in the Southern hemisphere has a maximum of 9-10s off of the South West African coast during the summer months (Young, 1999). The North Sea, Mediterranean and the Caribbean Sea show a lower mwp than the surrounding open water all year round. The tropical East Pacific has a very high mwp with its lowest of 9.5s in September and its highest values of 12s in May.

The whole basin shows variability throughout the year (**ERA40_mwp_anom.mov**). From September 1992 - June 1993 a large decrease in mwp can be observed across the whole region of the North Atlantic. After June 1993 a large increase in mwp occurs off of the east coast of America with an increase of 2s which extends eastwards until December 1993. In December 1998 there is a large decrease in mwp in the north east region of -1.5s. December 2000 shows a decrease in mwp in the eastern region.

The short ERA-Interim dataset shows a lower mwp for a small area in the Pacific region by 1-2s in October compared with the ERA-40 dataset (**ERAint_mwp_clim_short.mov**). This area is even larger in size during November and December up to 3s. The increased resolution is likely to have resolved the Galapagos Islands and its effect in decreasing mwp. Much lower values can be observed in coastal regions. In February the mwp of approximately 10s extends slightly more westward than the ERA-40 values in the Central North Atlantic and the larger

mwp values extend from the North West African coast into the North Atlantic further in the ERA-Interim dataset in May. The summer months are similar in both model datasets.

The differences in anomalous months are very large at the start of the time series between ERA-40 and ERA-Interim (**ERAint_mwp_anom_short.mov**). The largest difference occurs in the first few years from September 1992 - 1995 Here ERA-Interim gives larger values of up to 2 s and slightly different spatial patterns. However, ERA-Interim does give some lower values such as at the start of 1996. From 1998 onwards the models do not diverge so much in terms of spatial patterns but ERA-Interim still gives slightly larger positive anomalies.

The mwp monthly climatologies from ERA-Interim September 1992 - July 2009 (**ERAint_mwp_clim.mov**) shows little difference from the earlier time period of September 1992 – August 2002 in contrast to the clear changes observed in wind speed and swh between the two time periods.

The monthly anomalies are shown in **ERAint_mwp_anom.mov.** In winter 2003/2004 the eastern region is highly variable as the values alternate from a large decrease of 1.5 s in November to an increase of 1.5 s in December 2003, followed by a low of 1-1.5 s in the western region. February 2005 shows a large increase in mwp of 1.8 s in the eastern region where as March 2005 shows an extreme low of -2 s in the central region. February 2007 also shows a large decrease in mwp in the northern region of -2 s.

The std of the monthly climatologies can be found in **ERAint_mwp_std.mov**. The summer months give the lowest std in the North Atlantic throughout the year with values less than 0.5s. December shows the greatest variability in the east as std reaches 1 s and February shows a high std area around Spain. Hudson Bay and west of Greenland show spurious data. The results are similar to Sterl and Caires (2005) who studied 1971-2000 with the 1.5° x 1.5° 3 hour ERA-40 dataset with only subtle changes in location of maximum mwp, such as the

maximum shifts slightly northwards from outside the Strait of Gibraltar in February of the recent time period.

4.1.5. Altimeter T_z

Before a comparison is made between the satellite and the model is it worth noting the subtle differences in the wave period measured. The model provides mwp defined as T_e where as the satellites measure T_z (**Appendix. 1.**). T_e is slightly larger than T_z as it is dependant of the form of the spectrum (Mackay *et al*, 2008). The climatology of T_z from the short TOPEX data is given in **tx_tz_clim_short.mov**. The data shows a large change in the mwp for the entire North Atlantic in the winter. The results are much smaller in the North East Atlantic and Pacific region with a maximum of 10s in January. The model data does not show as strong latitudinal variation of wave period compared to the satellite data. The summer months also show that the model data overestimates the wave period. The anomalous months are given in **tx_tz_anom_short.mov**. These are in fairly good agreement to the model data showing the annual changes in mwp from the models are relative (**ERAint_mwp_anom_short.mov**).

The tx-j1 T_z climatology is shown in **tx_j1_tz_clim.mov.** The maximum T_z in the winter months from the later time series dataset is ~0.3s less than the earlier TOPEX dataset, showing a calmer wave climate in recent winter months, whereas, all other months are similar. The monthly anomalies are given in **tx_j1_tz_anom.mov**.

The e2-n1 T_z climatology is given in **e2_n1_tz_clim.mov** and the monthly anomalies in **e2_n1_tz_anom.mov**. The results between the different satellite datasets show tx-j1 gives slightly larger maximum T_z results of approximately 0.1-0.2s in July, August, September and

October. In December, e2-n1 gives slightly larger maximum T_z values, whereas in January, February and March tx-j1 gives marginally larger results. The anomalous months also show observable changes throughout the entire time series and show more spurious data in the great lakes in the e2-n1 data.

Swell conditions dominate the north and east regions of the North Atlantic. Wave period is greater in the east as the westerly winds across the North Atlantic have time to build up and create longer swell waves. The phase of the NAO influences the direction of winds and storm tracks in the winter months which increases wave period (Rogers, 1997).

The results from this study show the mwp of ERA-40 and ERA-Interim are much larger than that obtained from satellite data by 1-2 in the East Atlantic. However, The mwp results are much larger than previous ERA-40 data used (Sterl and Caires *et al*, 2005) as their January climatology from the 1971-2000 period has a maximum of 9 s. Caires *et al* (2005) used the full ERA-40 dataset against the mean wave period (T_m) (**Appendix. 1.**) from altimeters for a global comparison with a resolution of 1.5° x 1.5°. They found that ERA-40 actually has a tendency to underestimate mwp in the North Atlantic and the highest errors occurred in the tropics. Previous comparisons against satellite data also highlight the large mwp values I obtained (Sykes, 2005). The free online dataset may possibly be giving larger mwp values in comparison to the full version with a 1.5° x 1.5° resolution.

The large errors of mwp at the start of the time series until May 1993 are likely to have been caused by the faulty FDP (December 1991-May 1993) of ERS-1. The lowest route-mean-square-error (rmse) mwp values with comparison to buoy data were obtained between January 1994 and May 1996 due to an uncalibrated FDP of ERS-1. After June 1996 ERS-2 FDP is assimilated, which improved the wave field in the tropics (Sterl and Caries, 2005).

4.2. EOFs

4.2.1. ERA wind speed

The first 4 EOFs of wind speed from ERA-40 explain 13.4%, 8.5%, 5.8% and 5.5% of the variance, respectively (**Figure. 4.2.1.**). The first EOF shows a tri-pole structure from approximately 10°N to 60°N with a slight north east to south west tilt. The second EOF shows variability in the north east as a minimum can be seen at 40°N, 20°W, and a maximum in the very north east of the plot, a north-south dipole. There is also a slight minimum around 10°N.

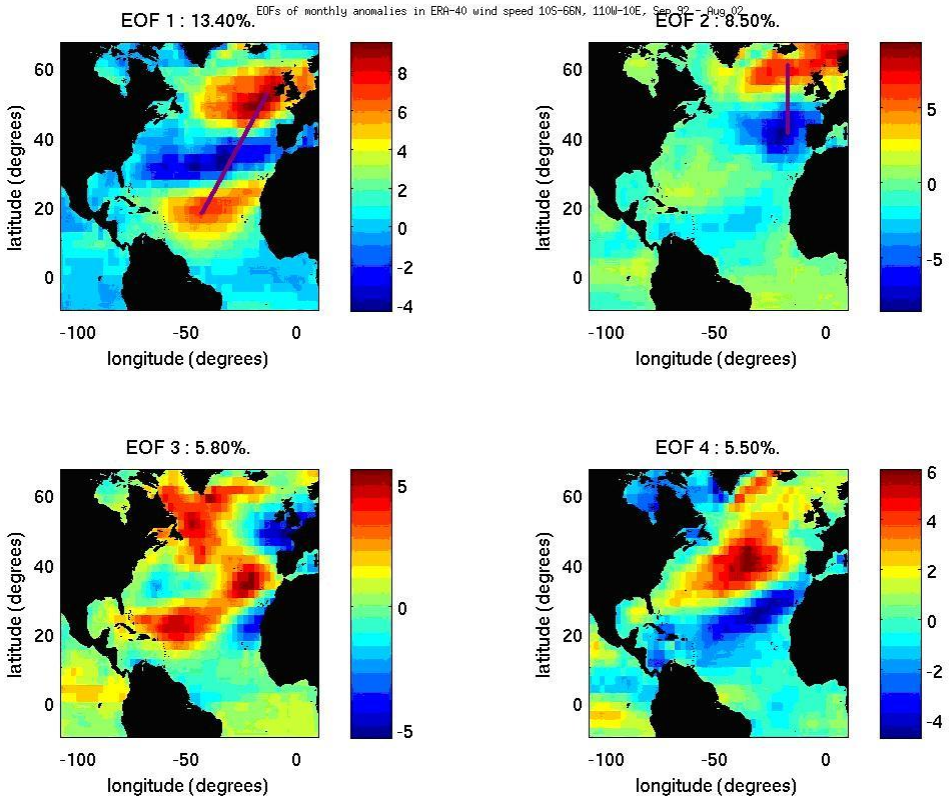

Figure. 4.2.1. The first 4 EOFs in ERA-40 wind speed 10°S-66°N, 110°W-10°E, September 1992 – August 2002

ERA-40 1992-2002	NAO	EAP
PC1	**0.52**	**0.46**
PC2	**0.35**	**-0.25**

Table. 4.2.1. Cross-correlation coefficient (r) between climate indices NAO (North Atlantic Oscillation) and EAP (East Atlantic Pattern) for the principal components of the two leading EOFs. Values of r in bold are statistically significant at the 5% significance level (i.e. 95% confidence level).

The first PC associated with the first EOF of ERA-40 wind speed has a strong correlation with the NAO (**Table. 4.2.1.**). It is also correlated quite high with the EAP and both are significant at the 95% confidence level. The second PC also has more of an influence from the NAO than the EAP. It should be noted the correlation between NAO and EAP is approximately 0.1.

The first 4 EOFs of wind speed from ERA-Interim September 1992 – August 2002 explain 13.5%, 8.9%, 6.2% and 6% of the variance, respectively (**Figure. 4.2.2.**). The values are very similar between both models and all show similar patterns.

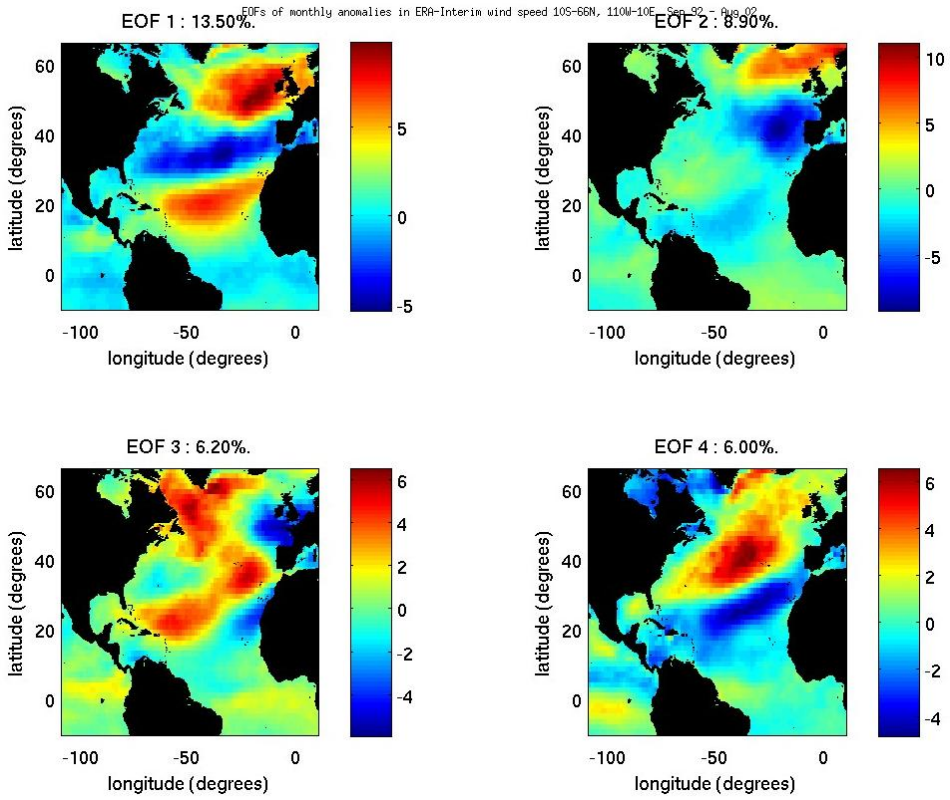

Figure. 4.2.2. The first 4 EOFs in ERA-Interim wind speed 10°S-66°N, 110°W-10°E, September 1992 – August 2002

ERA-Interim 1992-2002	NAO	EAP
PC1	**0.53**	**0.46**
PC2	**-0.39**	**0.31**

Table. 4.2.2. Cross-correlation coefficient (r) between climate indices NAO (North Atlantic Oscillation) and EAP (East Atlantic Pattern) for the principal components of the two leading EOFs.

The correlations of the PCs associated with these EOFs against climate indices are similar to ERA-40 (**Table. 4.2.2.**). There are slightly stronger correlations of the second PC with the atmospheric modes compared to the ERA-40 data.

The first 4 EOFs of wind speed from the full ERA-Interim dataset explain 12.8%, 8.3%, 5.3% and 4.9% of the variance, respectively (**Figure. 4.2.3.**). Note the change of sign in EOF 2 is arbitrary and in this case the negative value is placed with the PC instead.

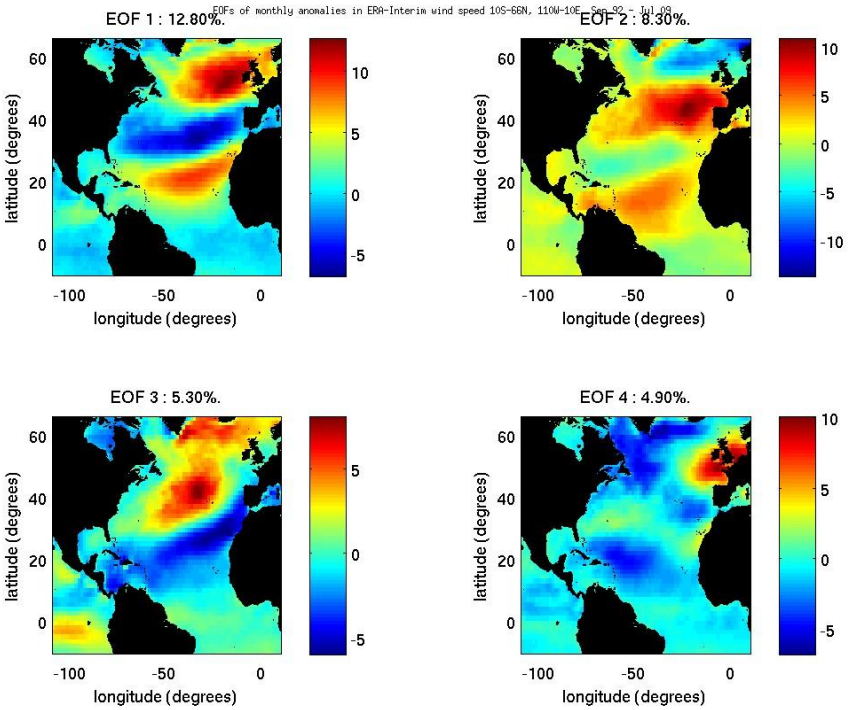

Figure. 4.2.3. The first 4 EOFs in ERA-Interim wind speed 10°S-66°N, 110°W-10°E, September 1992 – July 2009

ERA-Interim 1992-2009	NAO	EAP
PC1	**0.49**	**0.38**
PC2	**-0.39**	**0.31**

Table. 4.2.3. Cross-correlation coefficient (r) between climate indices NAO (North Atlantic Oscillation) and EAP (East Atlantic Pattern) for the principal components of the two leading EOFs.

Correlation of the first PC slightly declines against the atmospheric modes for the longer timer series (**Table. 4.2.3.** and **Figure. 4.2.4.**). The second PC is similarly correlated with the atmospheric modes as shorter time series (**Figure. 4.2.5.**).

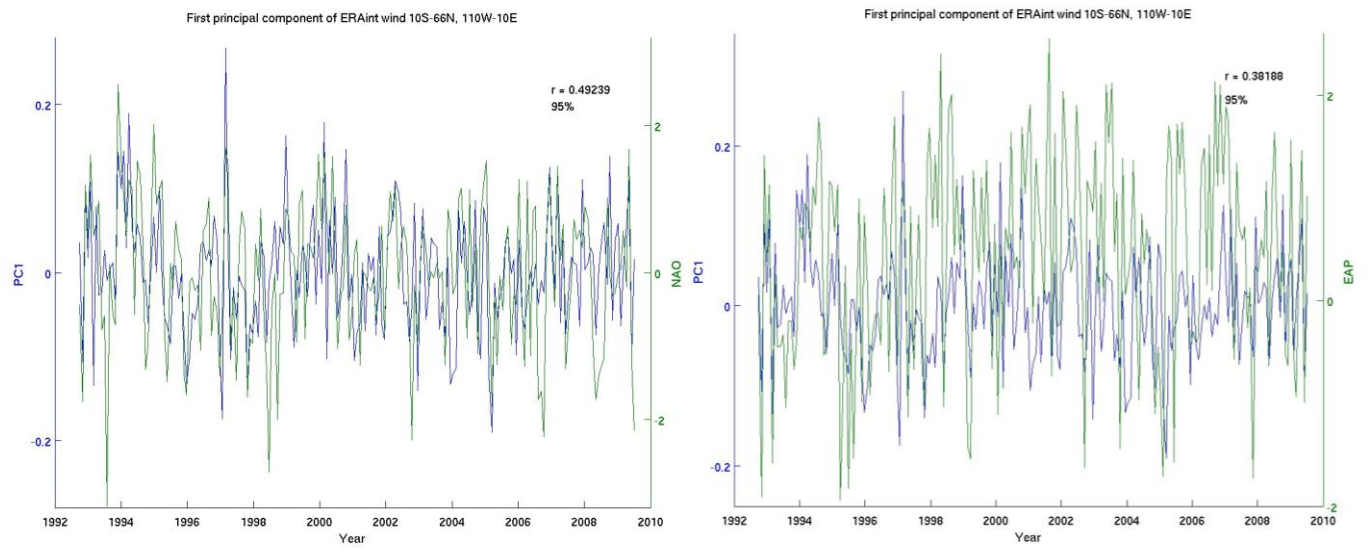

Figure. 4.2.4. Left, correlation of PC1 against NAO. Right, correlation against EAP

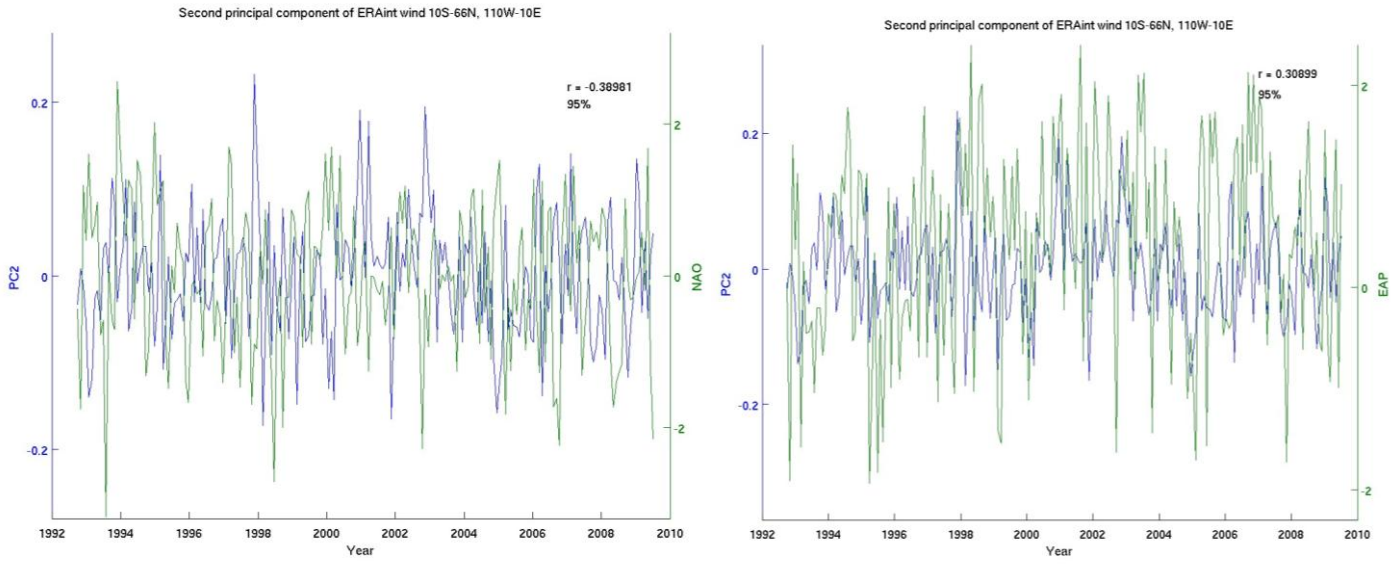

Figure. 4.2.5. Left, correlation of PC2 against NAO. Right, correlation against EAP

The variability of the wind field shows a little more influence from the NAO than the EAP for the first two EOFs but does not separate these atmospheric forcings. The spatial pattern of the first EOF shows a typical NAO like tri-pole. The results are very similar to Sterl and Caires (2005) who use the 1.5° x 1.5° ERA-40 data set for the whole time-series (1957-2002) and also notice the slight north east south west tilt of the tri-pole, however their first EOF

explained more variance at 17.6%, possibly due to their more north eastward spatial area studied (80°N-0°N, 70°W-20°E). The spatial patterns are also comparable to Sykes (2005) who used altimeter data. He similarly found variance explained by the first EOF of 19%, but only studied the winter months and no further south than the Equator. Cotton *et al* (1997) found the PC of the first EOF mode to be correlated with the NAO with r = 0.78 also using the winter months and a slightly smaller area. Sykes (2005) was able to separate the NAO with the first EOF and the EAP with the second EOF. The spatial pattern for my second EOF is similar to Sterl and Caires (2005) but does not show such a marked north east – south west quad-pole. Again the second EOF explains a smaller percent of the variance in comparison to Sykes (2005) and Sterl and Caires (2005), as they calculate 11.3% and 12% respectively.

4.2.2. ERA swh

The first 4 EOFs of ERA-40 swh explain 31.8%, 18%, 11.9% and 7.4% of the variability, respectively (**Figure. 4.2.6.**). The spatial pattern of the first EOF shows a maximum to the west of the British Isles. The second EOF shows a strong north east – south west dipole located in the north east region. The positive area is located north of the British Isles and the minimum area is to the west of Spain.

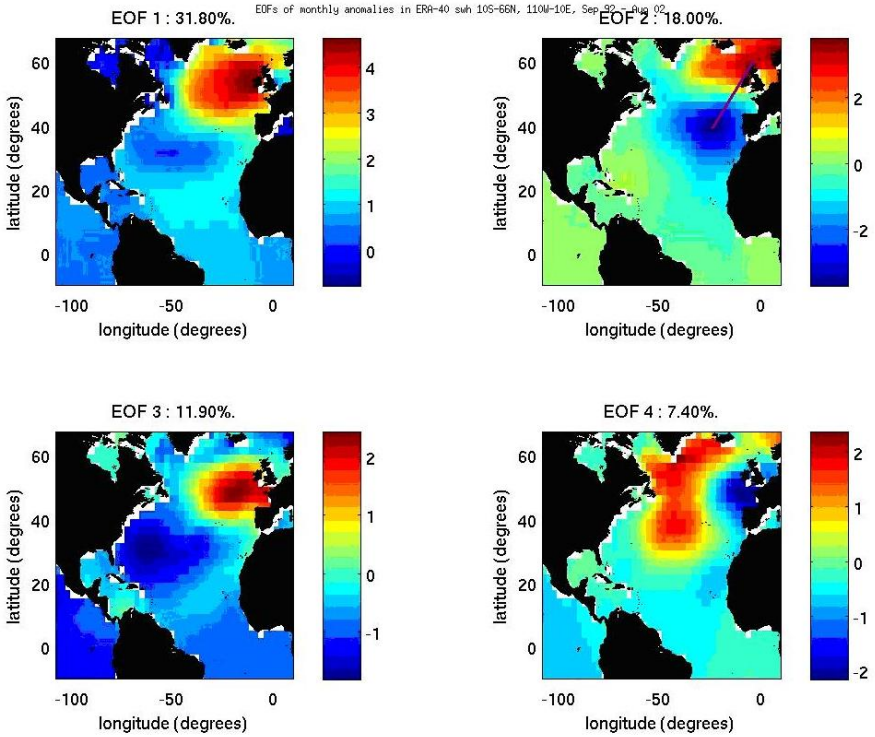

Figure. 4.2.6. The first 4 EOFs in ERA-40 swh 10°S-66°N, 110°W-10°E, September 1992 – August 2002

ERA-40 1992-2002	NAO	EAP
PC1	**0.37**	**0.41**
PC2	**0.41**	**-0.2**

Table. 4.2.4. Cross-correlation coefficient (r) between climate indices NAO (North Atlantic Oscillation) and EAP (East Atlantic Pattern) for the principal components of the two leading EOFs.

The first PC is similar to wind speed and has high correlations with both the EAP and NAO, but the EAP is slightly stronger (**Table. 4.2.4.**). The second PC has a strong link with the NAO and is greatly reduced for the EAP.

The first 4 EOFs of swh from the ERA-Interim September 1992 – August 2002 dataset explain 30.4%, 21.1%, 9.7% and 5.2% of the variance, respectively (**Figure. 4.2.7.**). The variances explained are similar to ERA-40 with a slight increase in the second EOF of 3%. The spatial patterns for the first two EOFs are similar whereas the spatial pattern of the third

EOF in the ERA-Interim model is similar to the fourth EOF of ERA-40. The fourth EOF of ERA-Interim gives a new pattern of variability.

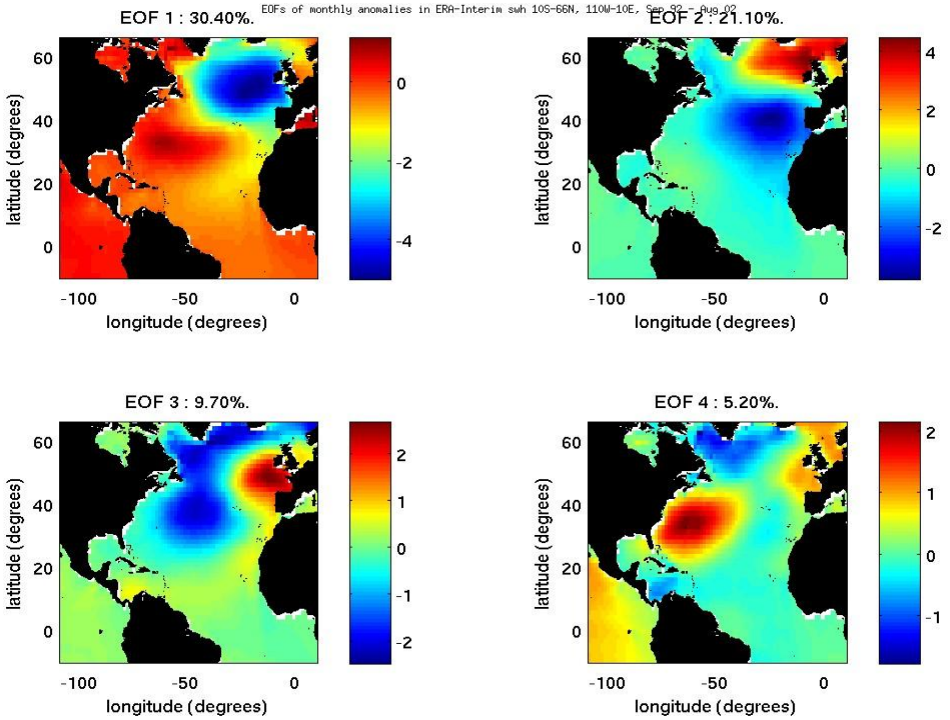

Figure. 4.2.7. The first 4 EOFs in ERA-Interim swh 10°S-66°N, 110°W-10°E, September 1992 – August 2002

ERA-Interim 1992-2002	NAO	EAP
PC1	**-0.38**	**-0.5**
PC2	**0.41**	**-0.2**

Table. 4.2.5. Cross-correlation coefficient (r) between climate indices NAO (North Atlantic Oscillation) and EAP (East Atlantic Pattern) for the principal components of the two leading EOFs.

The first PC of swh from the ERA-Interim dataset has a stronger correlation to the EAP than ERA-40 by 0.09 (**Table. 4.2.5.**). The second PC has a stronger correlation with the NAO than ERA-40 and a weaker correlation with EAP**.** Suggesting that ERA-Interim is forced by the atmospheric modes present more accurately than ERA-40.

The first 4 EOFs from the full ERA-Interim dataset of swh explain 30.8%, 20.8%, 8.3% and 4.8% of the variance, respectively (**Figure. 4.2.8.**). The spatial patterns of the first 4 EOFs are very similar with the shorter time scale.

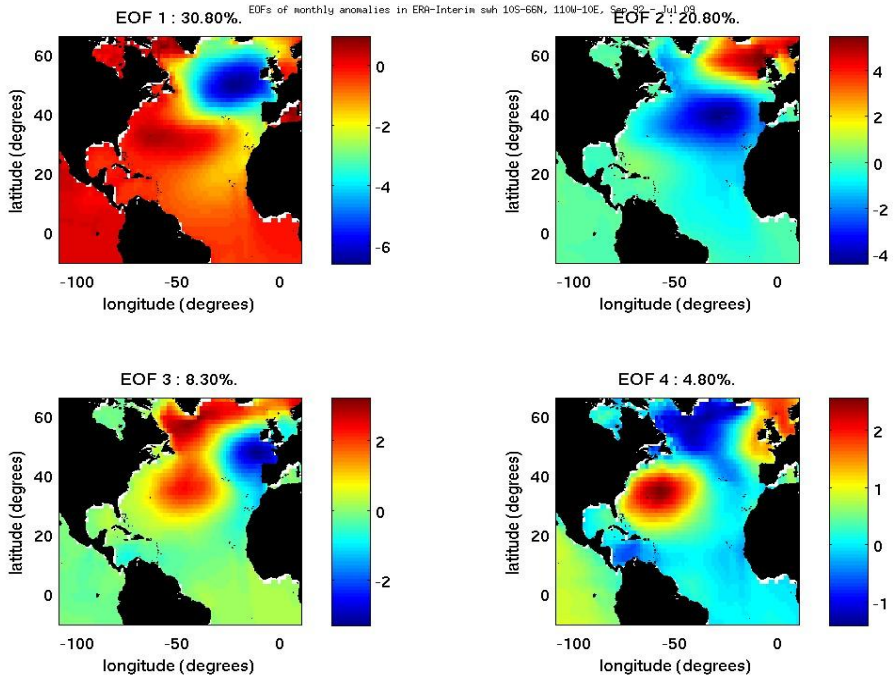

Figure. 4.2.8. The first 4 EOFs in ERA-Interim swh 10°S-66°N, 110°W-10°E, September 1992 – July 2009

ERA-Interim 1992-2009	NAO	EAP
PC1	**-0.25**	**-0.5**
PC2	**0.55**	**-0.11**

Table. 4.2.6. Cross-correlation coefficient (r) between climate indices NAO (North Atlantic Oscillation) and EAP (East Atlantic Pattern) for the principal components of the two leading EOFs.

The first PC has a similar strong correlation with EAP; however its correlation with the NAO is reduced compared to the shorter time span (**Table. 4.2.6.** and **Figure. 4.2.9.**). This suggests that the NAO's forcing on the major variability of the wave field has reduced in recent times and the EAP's influence has increased (Sykes, 2005). The positive phase of the EAP was

particularly strong and persistent during 1997-2004, when 3-month running mean values routinely averaged 1.0-2.0 standard deviations above normal (NOAA CPC, 2008). The second EOF has a similar correlation with the NAO of **r = 0.55** and the EAP **r = -0.11** (**Figure. 4.2.10.**).

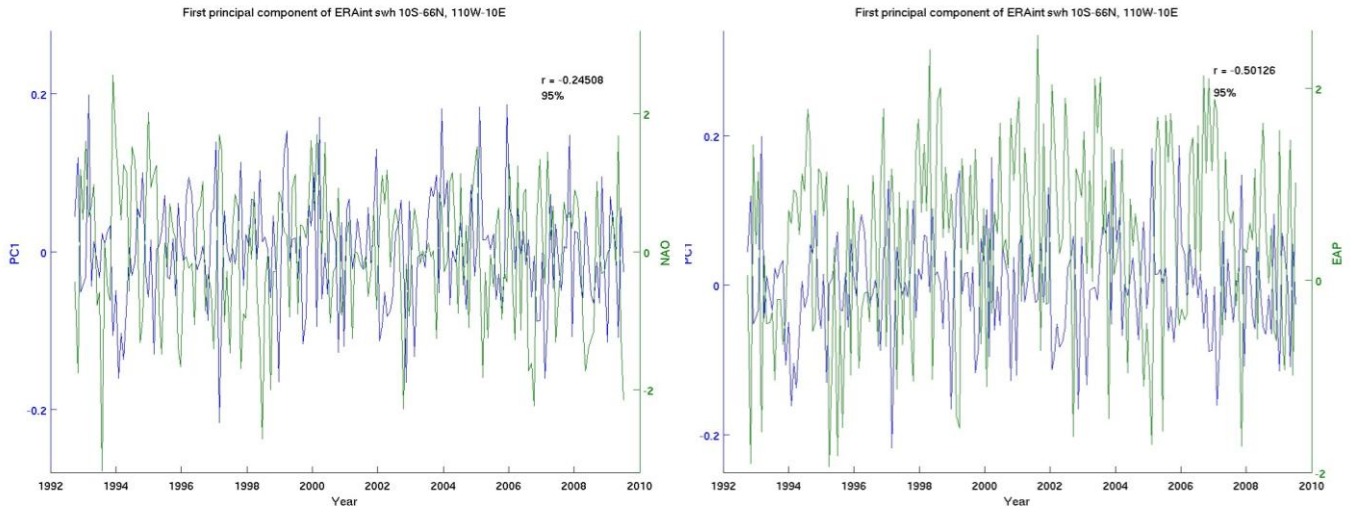

Figure. 4.2.9. Left, correlation of PC1 against NAO. Right, correlation against EAP

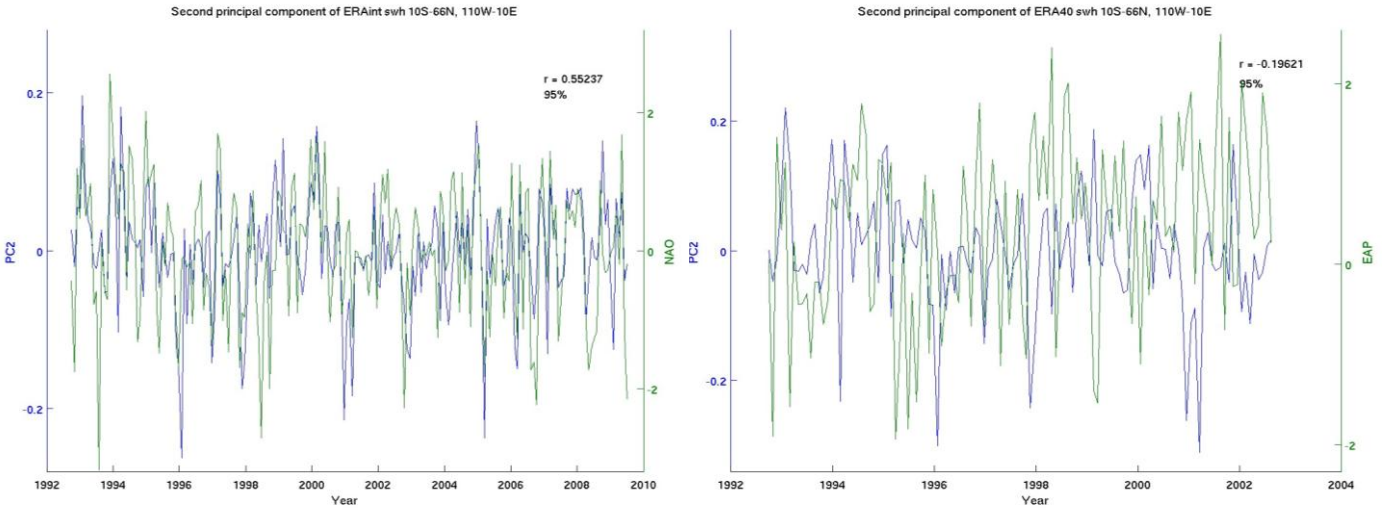

Figure. 4.2.10. Left, correlation of PC2 against NAO. Right, correlation against EAP

4.2.3. Altimeter swh

The first 4 EOFs for swh from the shortened TOPEX dataset of January 1993 – August 2003 are shown in **Figure. 4.2.11**. The EOFs still show trackiness which is observed in the data. The percentage variance of the first EOF explained is 10% less than the ERA-Interim data of a similar time period at 21.6%; however the spatial pattern is similar. The second EOF explains 7% less of the variability at 13%, and shows a similar spatial pattern. The third EOF shows a reduction in the variability explained, showing the satellite data is picking up more modes of variability as the variance is likely to be increase at higher modes. The fourth EOF although explaining a similar percentage variance, gives a different spatial pattern.

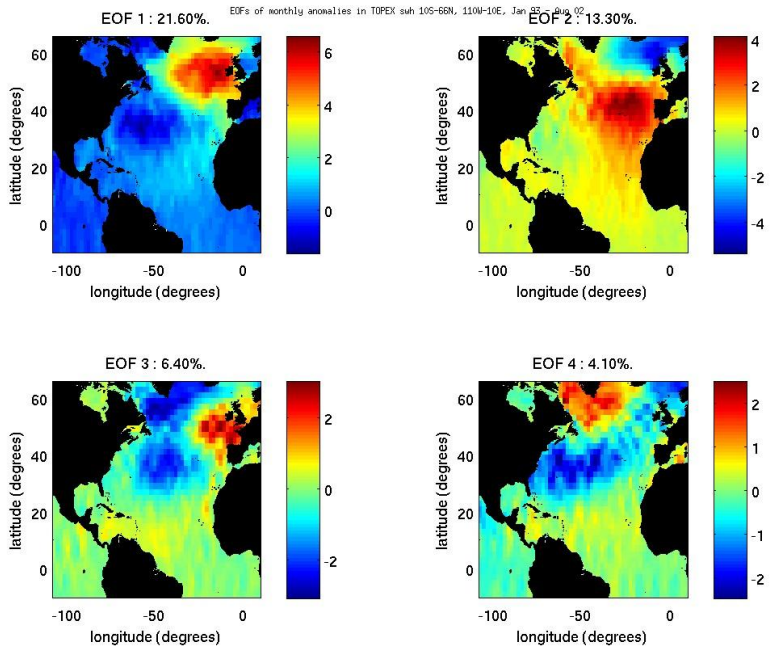

Figure. 4.2.11. The first 4 EOFs in TOPEX swh 10°S-66°N, 110°W-10°E, January 1993 – August 2002

TOPEX 1993-2002	NAO	EAP
PC1	**0.35**	**0.41**
PC2	**-0.42**	**0.14**

Table. 4.2.7. Cross-correlation coefficient (r) between climate indices NAO (North Atlantic Oscillation) and EAP (East Atlantic Pattern) for the principal components of the two leading EOFs.

The first PC has a fairly similar correlation with the NAO but gives a slightly weaker correlation for the EAP by 0.09 compared to ERA-Interim September 1992 – August 2002 (**Table. 4.2.7.**). The second PC is correlated against the NAO less than the correlation in ERA-Interim by 0.13. The correlation against the EAP is only slightly different.

The first 4 EOFs from tx-j1 show the percentage variance explained are fairly similar to the shorted TOPEX data, however, the fourth EOF gives a slightly different spatial pattern (**Figure. 4.2.12**.).

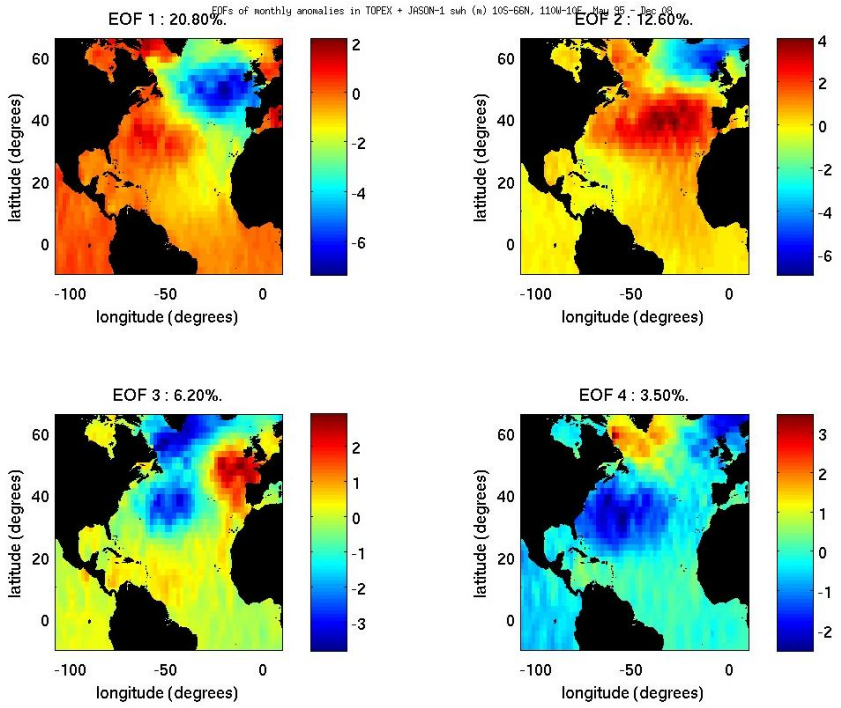

Figure. 4.2.12. The first 4 EOFs in TOPEX + Jason-1 swh 10°S-66°N, 110°W-10°E, May 1995 – December 2008

TOPEX + Jason-1 1995-2008	NAO	EAP
PC1	**0.08**	**-0.58**
PC2	**-0.48**	**0.08**

Table. 4.2.8. Cross-correlation coefficient (r) between climate indices NAO (North Atlantic Oscillation) and EAP (East Atlantic Pattern) for the principal components of the two leading EOFs.

The correlation of the first PC against NAO is greatly reduced in this longer series satellite data compared to the earlier TOPEX data (**Table. 4.2.8.**), whereas NAO's correlation with PC2 has greatly increased. The correlation of PC1 against the EAP is only slightly larger and is slightly reduced against PC2. This implies the NAO has gone into a more negative phase in recent years as it now has more of an influence on the second mode of variability or the EAP has gone into a more positive phase and controls the main patterns of the wave parameters as it dominates the first mode of variability.

In comparison to the tx-j1 satellite data the first 4 EOFs for e2-n1 are given in **Figure. 4.2.13**. The e2-n1 shows slightly more trackiness. There is a slight reduction of the second EOF to 10.5%. The spatial patterns are fairly similar with only subtle differences in EOF 4.

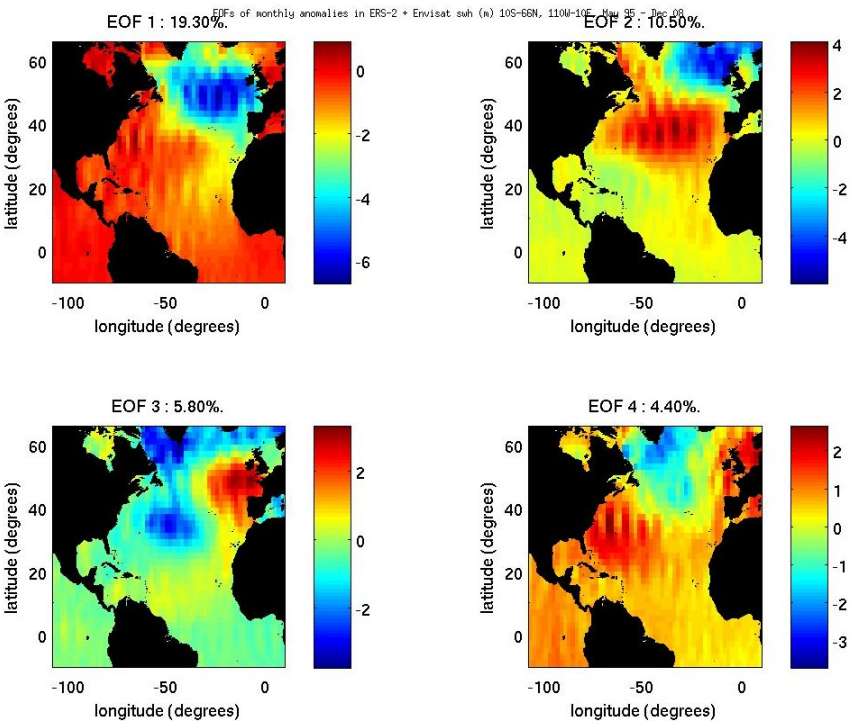

Figure. 4.2.13. The first 4 EOFs in ERS-2 + Envisat swh 10°S-66°N, 110°W-10°E, May 1995 – December 2008

ERS-2 + Envisat 1995-2008	NAO	EAP
PC1	**0.001**	**-0.63**
PC2	**-0.48**	**0.02**

Table. 4.2.9. Cross-correlation coefficient (r) between climate indices NAO (North Atlantic Oscillation) and EAP (East Atlantic Pattern) for the principal components of the two leading EOFs.

Although the spatial patterns are the same there are observable differences in the correlation against the atmospheric modes. PC1 is less correlated with the NAO and PC2 is more correlated with the NAO (**Table. 4.2.9.**). The EAP is similarly correlated with PC1 but less with PC2. This shows the swh from the e2-n1 dataset are separating these two atmospheric modes better than tx-j1.

Specific studies of investigating swh variability in the North Atlantic with its relation to the NAO have previously used only the winter months (Dec, Jan, Feb and Mar) and a smaller region of 30°N–66°N, 80°W–10°E (Woolf *et al*, 2002). This gave a very high first EOF of 41% and strong PC correlation with the Gibraltar-Iceland NAO index of r = 0.83. By observing an increased area of the Northern Atlantic the first 2 EOFs decreased the variance explained for both the model data and satellite data. Sykes (2005) also studied the winter months from 1992-2004 and found that EOF 1 was correlated with the NAO and EOF 2 correlated with the EAP. As the area of study decreases to the North East Atlantic the influence of the NAO on the wave field becomes greater (Dodet *et al*, 2010). Results from Sterl and Caires (2005) who studied an area limited by the coordinates of 0°N-80°N, 70°W-20°E and the complete ERA-40 time series (1957 – 2002) obtained data showing the first EOF at 34.4%, with a peak situated at 45°N, 30°W and little variability for the rest of the basin with minor peaks in the North Sea and Mediterranean Sea. My research concurs with this pattern; they found the second EOF which explained 24% of the variance has a correlation of 0.8 with the NAO. Unfortunately they did not correlate the first EOF with any atmospheric modes.

However, as the area of study in the North Atlantic expands south westwards and if all months of the year are studied and the time series is extended into the late 2000s, it seems the EAP has a larger influence on the wave field than the NAO. The satellite data and full ERA-Interim data show that EOF 1 is more correlated with the EAP and EOF 2 with the NAO, although the magnitude of correlation of EOF 2 with the NAO is larger. This points out that the inter-annual variability of the EAP is larger than that of the NAO. There have only been a few recent studies which investigate the influence of the EAP on the North Atlantic wave field. Trigo *et al* (2008) and Lionello and Galati (2008) investigated the correlation of the EAP on the wave climate but not its influence on variability (see section **4.3.2.**). Semedo *et al*

(2009) showed that correlation of his swh EOF 2 reduced from 0.85 against the NAO using the winter months to 0.56 in the summer months.

4.2.4. ERA mwp

The first EOF of mwp from ERA-40 explains a large amount of the variability at 46.7% (**Figure. 4.2.14**.). The spatial pattern shows a low peak in Hudson Bay and a high peak in the south east of the plot while other areas show high variability. The subsequent 3 EOFs account for 15.5%, 7.9% and 6% of the variability respectively. The second EOF shows a low in the North East Atlantic and a high in the Pacific region divided by the land and the third EOF shows strong variability in the North Atlantic as a dipole with a dividing line from the tip of Greenland to the West Coast of Africa.

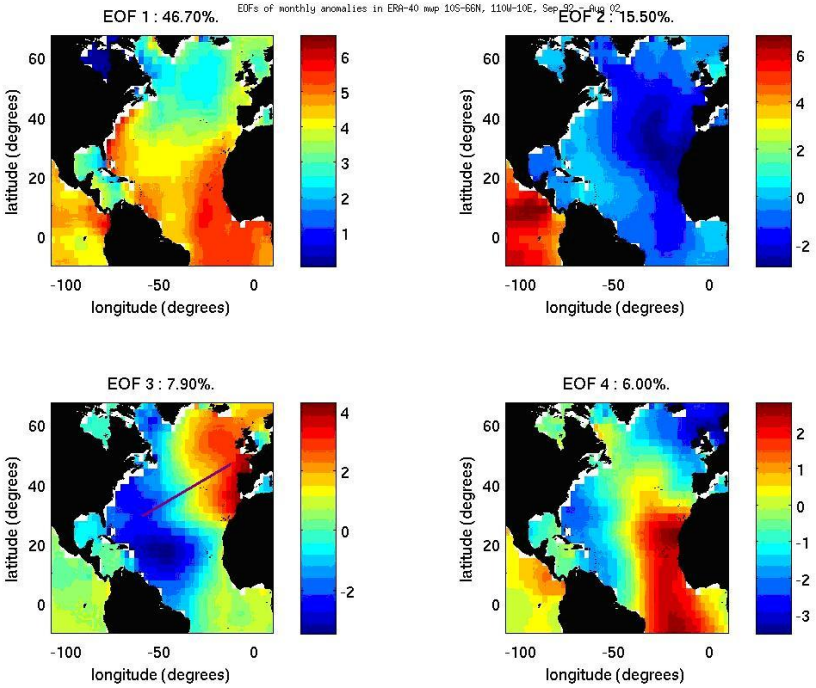

Figure. 4.2.14. The first 4 EOFs in ERA-40 mwp 10°S-66°N, 110°W-10°E, September 1992 – August 2002

ERA-40 1992-2002	NAO	EAP
PC1	**-0.02**	**0.1**
PC2	**-0.02**	**-0.08**
PC3	**0.47**	**0.37**

Table. 4.2.10. Cross-correlation coefficient (r) between climate indices NAO (North Atlantic Oscillation) and EAP (East Atlantic Pattern) for the principal components of the two leading EOFs.

The first and second PC of ERA-40 mwp have poor correlation with both the NAO and EAP (**Table. 4.2.10.**). The third PC has a NAO type spatial pattern and was therefore included in the correlation against the climatic indices.

The first EOF for mwp from the ERA-Interim September 1992 – August 2002 dataset explains 26.2% of the variability (**Figure. 4.2.15.**), 20% less than the first EOF from the ERA-40 dataset and it shows a similar spatial pattern to the second EOF of ERA-40. The second EOF of ERA-Interim shows a new spatial pattern and explains 16.4% of the variance, 1% more than ERA-40. The third EOFs are similar for both model datasets; however, ERA-Interim explains 14.2% of the variability, approximately 7% more. The fourth EOF shows a similar spatial pattern to the fourth EOF in ERA-40 and explains 8.7%.

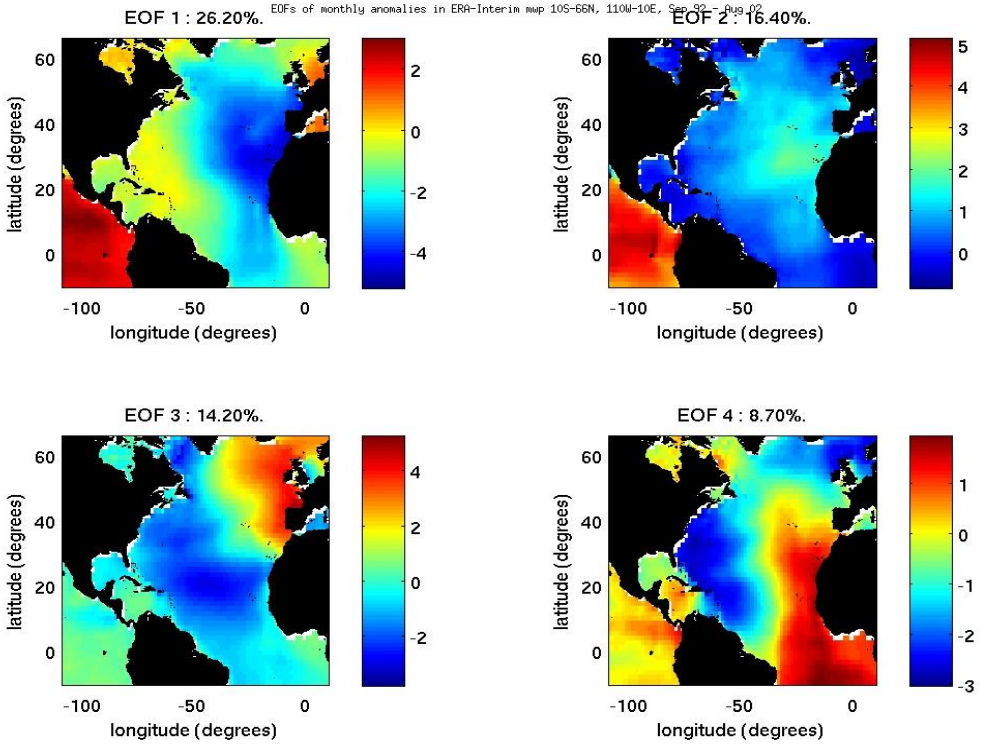

Figure. 4.2.15. The first 4 EOFs in ERA-Interim mwp 10°S-66°N, 110°W-10°E, September 1992 – August 2002

ERA-Interim 1992-2002	NAO	EAP
PC1	**-0.02**	**-0.25**
PC2	**-0.16**	**0.22**
PC3	**0.59**	**0.36**

Table. 4.2.11. Cross-correlation coefficient (r) between climate indices NAO (North Atlantic Oscillation) and EAP (East Atlantic Pattern) for the principal components of the two leading EOFs.

The first PC shows similar correlation with the NAO and is slightly enhanced with the EAP but is still relatively low compared to ERA-40 (**Table. 4.2.11.**). The second PC gives stronger correlations with the atmospheric modes than ERA-40 but is still low. PC 3 has a stronger correlation with the NAO and a similar correlation with the EAP.

The first EOF from the full ERA-Interim mwp dataset explains 28.9% of the variance (**Figure. 4.2.16.**). The spatial pattern of this first EOF shows a minimum in the Pacific region and a maximum in the central Eastern North Atlantic. It has a pattern similar to EOF 2 from the shorter time series, September 1992 – August 2002. The second EOF explains 15.5% of the variability. The third EOF explains 13% of the variability and shows a north east to south west dipole and a minimum in the North Sea. The fourth EOF explains 7.9% of the variability.

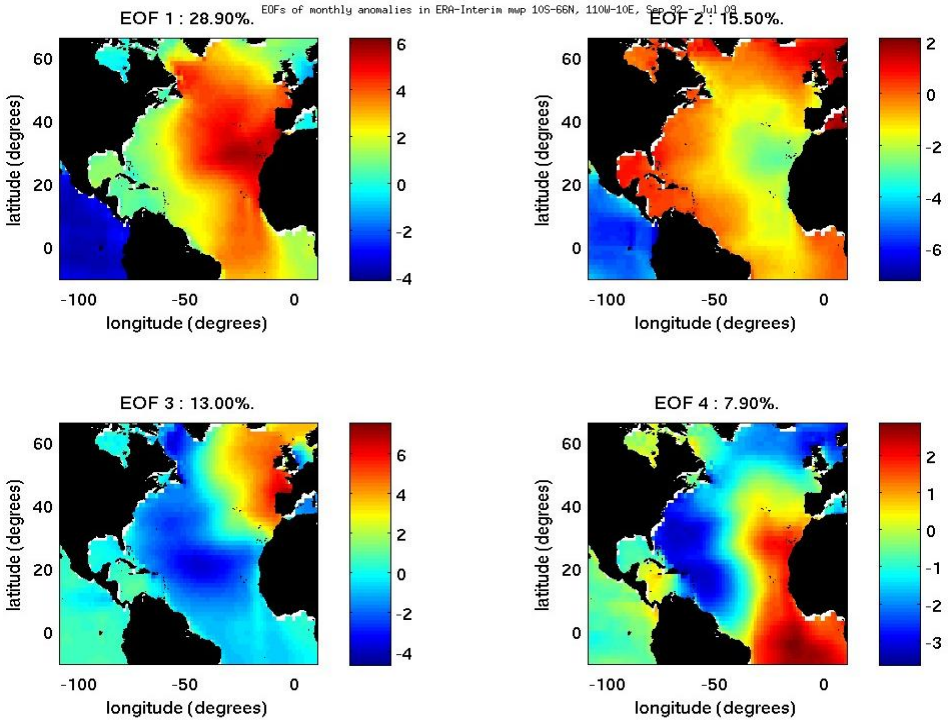

Figure. 4.2.16. The first 4 EOFs in ERA-Interim mwp 10°S-66°N, 110°W-10°E, September 1992 – July 2009

ERA-Interim 1992-2009	NAO	EAP
PC1	**-0.15**	**0.3**
PC2	**0.2**	**-0.32**
PC3	**0.56**	**0.32**

Table. 4.2.12. Cross-correlation coefficient (r) between climate indices NAO (North Atlantic Oscillation) and EAP (East Atlantic Pattern) for the principal components of the two leading EOFs.

Table. 4.2.12. shows the correlations of the first two PC with the atmospheric modes are still low (**Figure. 4.2.17.**). The third PC has slightly less correlation with the NAO and EAP as **r = 0.32** (**Figure. 4.2.18.**) compared to the shorter time series.

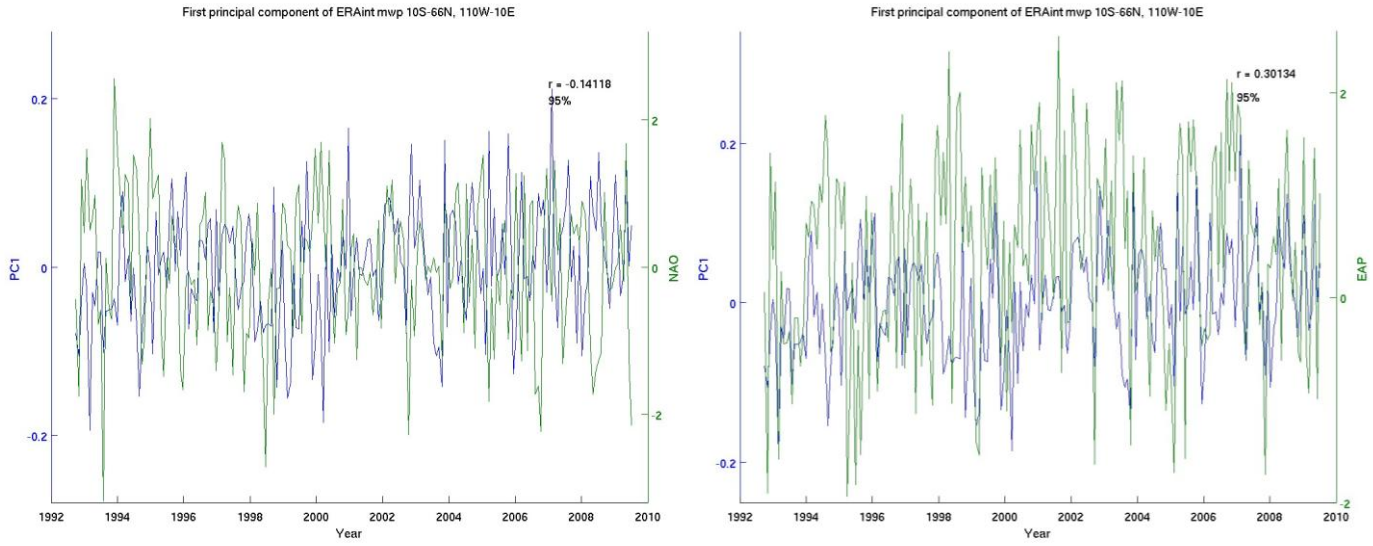

Figure. 4.2.17. Left, correlation of PC1 against NAO. Right, correlation against EAP

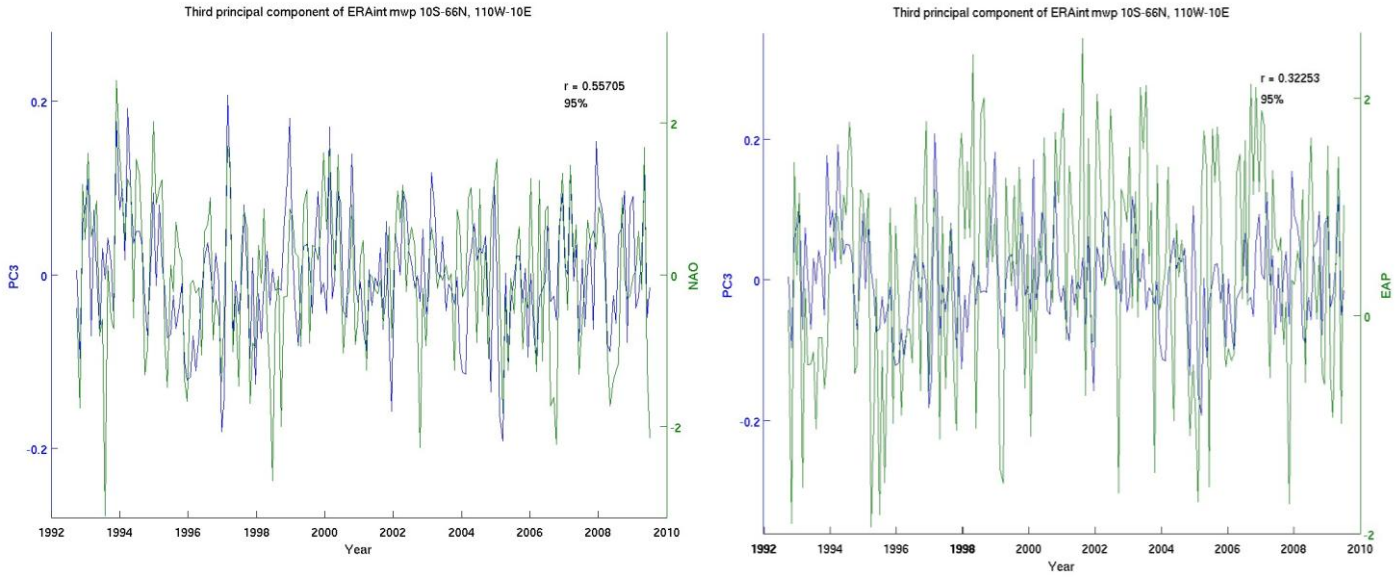

Figure. 4.2.18. Left, correlation of PC2 against NAO. Right, correlation against EAP

4.2.5. Altimeter T_z

The first 4 EOFs from the shortened TOPEX T_z explain 14.3%, 9.4%, 6.2% and 4.7% of variance, respectively (**Figure. 4.2.19.**), all much lower than the model data. The spatial pattern of EOF 2 looks similar to the third EOF from the model data.

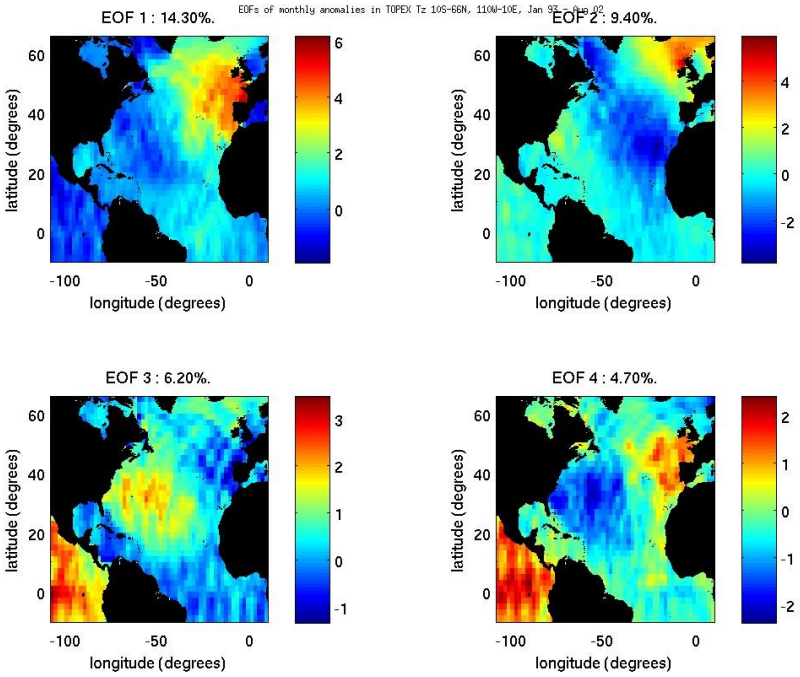

Figure. 4.2.19. The first 4 EOFs in TOPEX T_z 10°S-66°N, 110°W-10°E, January 1993 – August 2002

TOPEX 1993-2002	NAO	EAP
PC1	**0.26**	**0.41**
PC2	**0.52**	**0.01**
PC3	**-0.12**	**0.05**

Table. 4.2.13. Cross-correlation coefficient (r) between climate indices NAO (North Atlantic Oscillation) and EAP (East Atlantic Pattern) for the principal components of the two leading EOFs.

The first PC also has a similar correlation with the NAO but a much stronger correlation with the EAP compared to the model data (**Table. 4.2.13.**). The second PC has a much stronger

correlation with the NAO and a weaker correlation with the EAP. I also assessed the correlation of the third PC with the climate indices, similar to the study of the model data. These are much lower than the first two PCs as the climate indices already force the lower order EOFs. It is likely the satellite data are much more accurate as the results from the EOF analysis relate the wave period to the NAO and EAP similar to swh from the model and satellite data (see **section 4.2.2**.) whereas, the wave period given by the model does not.

The first EOF from tx-j1 explains 2% more of the variance at 16.3% **(Figure. 4.2.20.**) EOF 2 explain 1% less and EOF 4 shows a slightly different magnitude of its spatial pattern, otherwise the results are fairly similar to those of the TOPEX data.

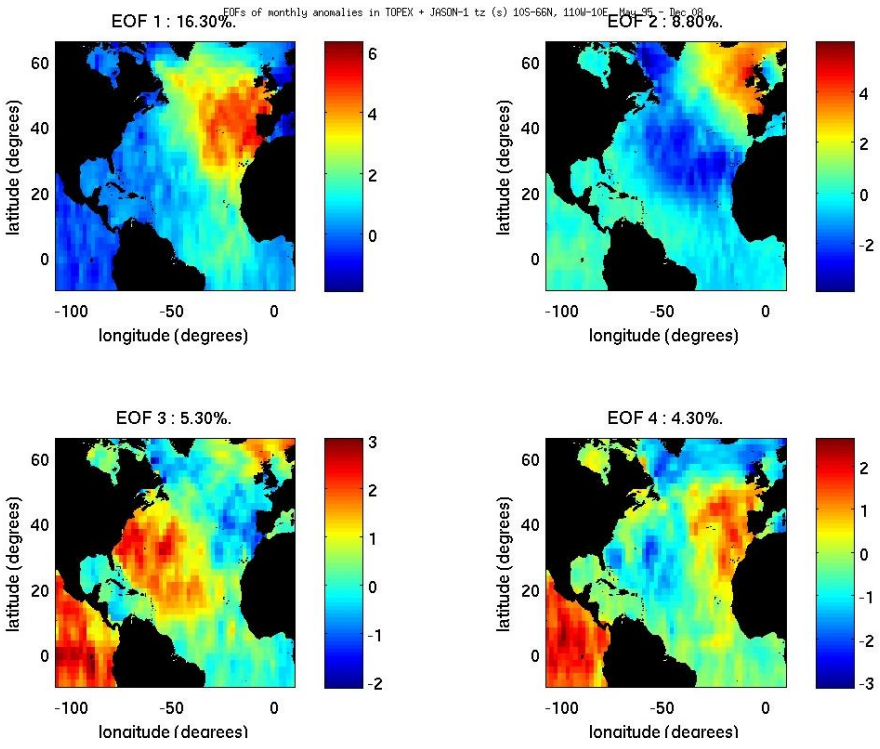

Figure. 4.2.20. The first 4 EOFs in TOPEX + Jason-1 T_z 10°S-66°N, 110°W-10°E, May 1995 – December 2008

TOPEX + Jason-1 1995-2008	NAO	EAP
PC1	**0.26**	**0.41**
PC2	**0.52**	**0.01**
PC3	**-0.12**	**0.05**

Table. 4.2.14. Cross-correlation coefficient (r) between climate indices NAO (North Atlantic Oscillation) and EAP (East Atlantic Pattern) for the principal components of the two leading EOFs.

The correlations for the first PC against the climate indices give a lower value against the NAO and a higher correlation against the EAP **(Table. 4.2.14.).** The second PC shows a stronger correlation with the NAO than the shorter TOPEX data set but also a slightly stronger correlation with the EAP. The third PC has poor correlation with the NAO and EAP.

For comparison with the 10 day sampling satellites of tx-j1, the e2-n1 data gives the first 4 EOFs of T_z in **Figure. 4.2.21**. The first EOF is much larger from e2-n1 and explains 39.2% of the variance and a completely different spatial pattern. The spatial patterns for EOF 2 and EOF 3 from e2-n1 are similar to EOF 1 and EOF 2 from tx-j1.

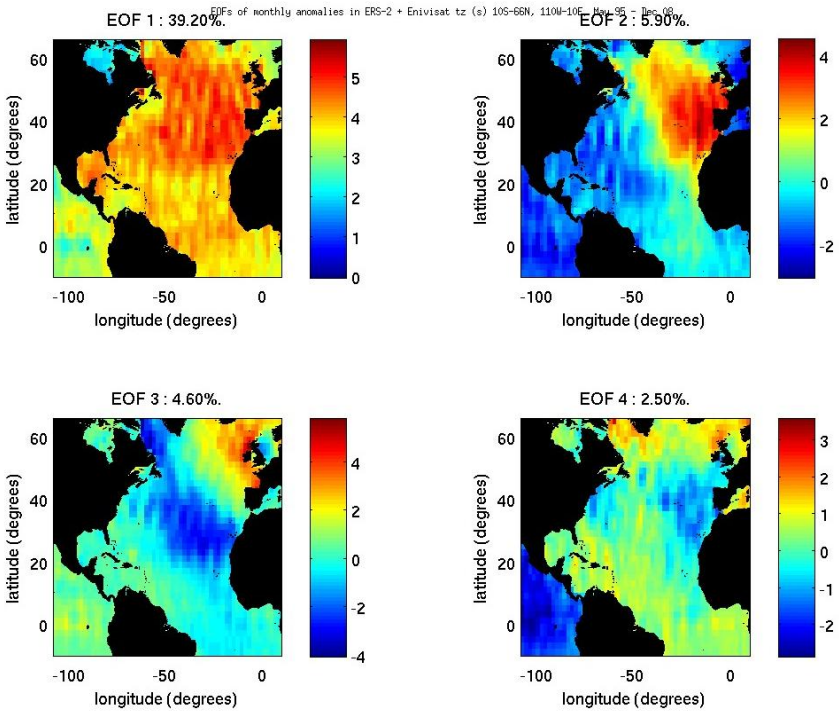

Figure. 4.2.21. The first 4 EOFs in ERS-2 + Envisat T_z 10°S-66°N, 110°W-10°E, May 1995 – December 2008

ERS-2 + Envisat 1995-2008	NAO	EAP
PC1	**-0.1**	**0.18**
PC2	**-0.04**	**0.41**
PC3	**0.6**	**0.12**

Table. 4.2.15 Cross-correlation coefficient (r) between climate indices NAO (North Atlantic Oscillation) and EAP (East Atlantic Pattern) for the principal components of the two leading EOFs.

The correlation of PC1 against the NAO and EAP are much lower compared to tx-j1 (**Table. 4.2.15.**). The second and third PC give strong correlation with the NAO and the EAP. These are more comparable to the first and second EOFs from tx-j1. The EOFs between the two satellite datasets show much larger differences for T_z compared to swh. The algorithm of T_z is based on swh but also the backscatter power, which is related to the wind speed. The greater temporal sampling of tx-j1 may be picking up the high frequency variability in the wind speed better than e2-n1. Observing the differences in wind speed from the satellite

datasets should highlight this difference as well. ERS-2 is a single frequency altimeter and therefore needs more quality checks when calibrated compared to the other dual frequency satellites. Further analysis is required to examine if both ERS-2 and Envisat are giving different T_z results, such as the negative T_z values in ERS-2 which were removed.

There have been few studies looking at the variability of wave period using an EOF analysis, however some have focused on the 100-year return value (Sterl and Caires, 2005) and the spatial variability of model and satellite data (Young, 1999b). Sykes (2005) studied T_z variability in the North Atlantic using altimeter data. He found his first EOF to explain 26% of the variance and a similar pattern to my second EOF from the TOPEX and tx-j1 data. The variance is stronger as the study period was over the winter months. His second EOF gave a variance of 22% and a similar pattern to my first EOF from the TOPEX and tx-j1 data. The wave period results from the most accurate TOPEX and tx-j1 data show there is more of an influence from the EAP than the NAO similar to swh, which has increased in recent years.

4.3. Spatial correlation of atmospheric modes

4.3.1. ERA wind speed

The spatial correlation images are similar to the spatial patterns of the respective EOF but give a more definitive correlation with the atmospheric mode. The NAO shows three clear zonal bands extending the width of the Atlantic at three different latitudes of alternating correlation (**Figure. 4.3.1.**). The main negative correlation band extends into the Mediterranean. Opposed to the spatial pattern of the EOF the correlation is fairly strong in the tropical West Atlantic as **r = 0.4**. This spatial correlation map looks similar to Sterl and

Caires (2005) first EOF but can also be related to the second EOF, as they are not greatly different. They also found a small patch of minimum variance on the Equator in both EOFs.

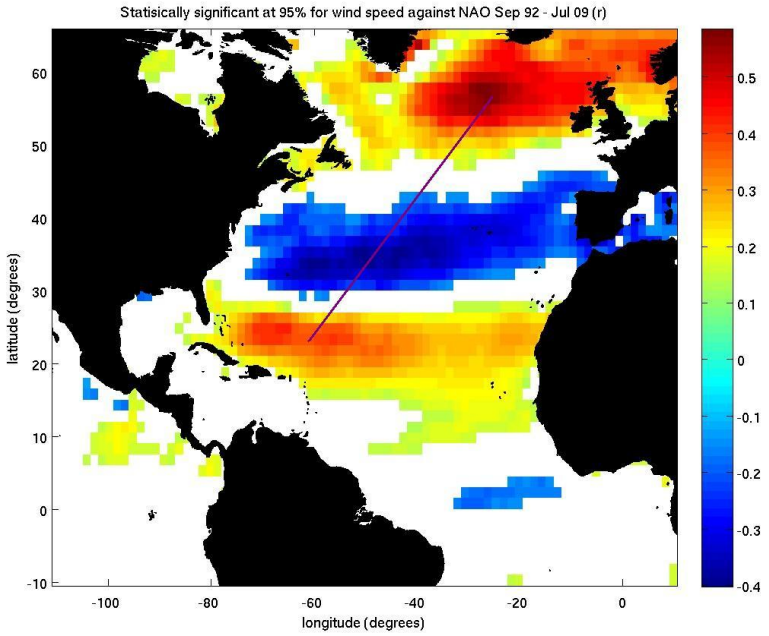

Figure.4.3.1. 95% Confidence level of wind speed anomalies against NAO anomalies from ERA-Interim September 1992 – July 2009

The relationship between the EAP and wind speed in the North Atlantic is shown in **Figure. 4.3.2.** Two large bands of positive correlation can be observed, both running from north east to south west. The strongest correlation is situated at 45°N, 28°W, with **r = 0.5**. Negatively correlated areas are small and widely distributed but the largest spatial regions are in the Mediterranean with **r = -0.25**. There are spurious data in the west and Hudson Bay.

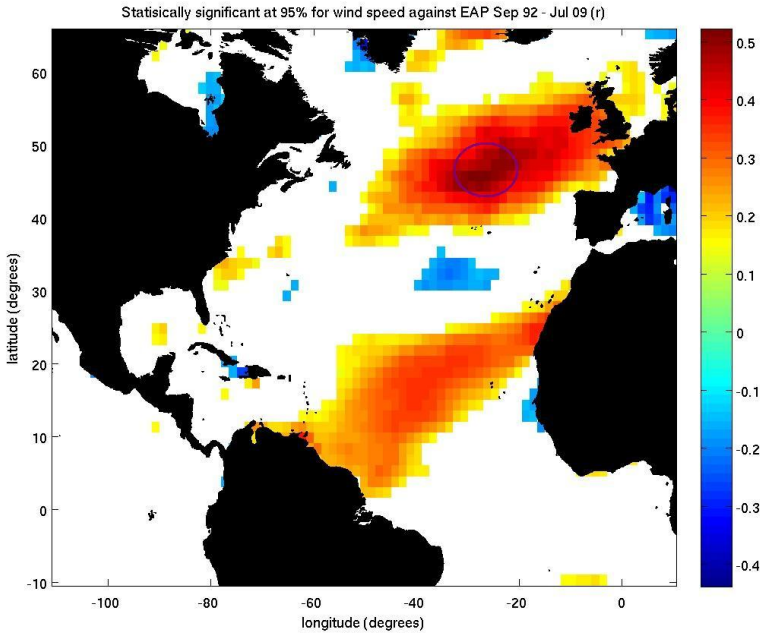

Figure. 4.3.2. 95% Confidence level of wind speed anomalies against EAP anomalies from ERA-Interim September 1992 – July 2009

The NAO and EAP both increase the wind speed at similar locations. The NAO gives stronger correlation but the EAP has a more coherent positive spatial configuration throughout the North Atlantic. Trigo *et al* (2008) also found the NAO had a stronger correlation than the EAP but the EAP had a stronger positive coherent pattern, however he only studied the extended winter months of October-March from 1960-2000 from the full ERA-40 dataset. In contrast, he only obtained one positive correlated band with the EAP, possibly due to the winter months studied and the study did not include the likely increase of the EAP's influence in recent years.

4.3.2. ERA swh

Figure. 4.3.3. shows swh from ERA-Interim is positively correlated with a maximum **of r = ~0.6** with the NAO to the north west of the British Isles. This is to the right of the maximum

located in the wind speed correlation. The maximum negative correlation occurs in the central North Atlantic as **r = -0.5**. The positively correlated areas in the west in the tropical North Atlantic and the small negatively correlated area on the Equator are similar to the wind speed.

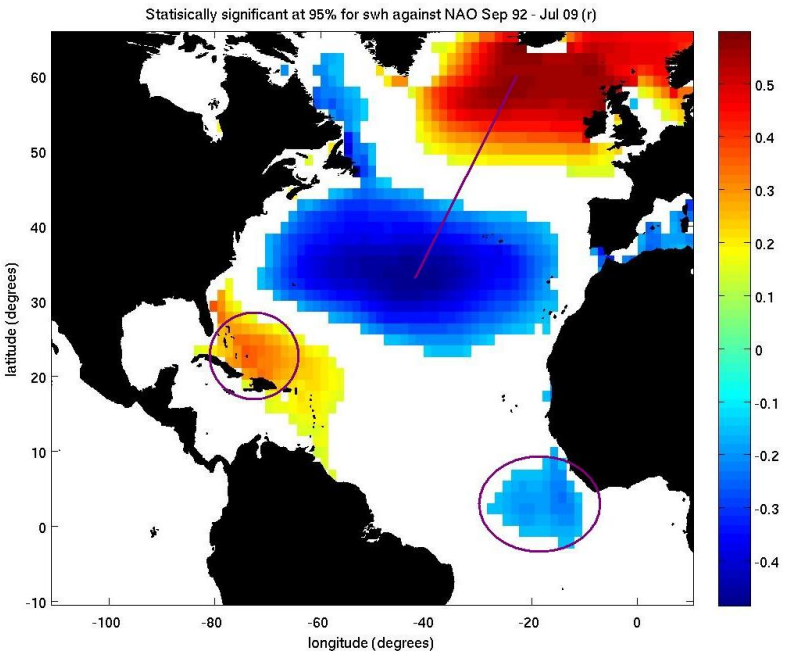

Figure. 4.3.3. 95% Confidence level of swh anomalies against NAO anomalies from ERA-Interim September 1992 – July 2009

The EAP has a positive correlation with the swh in the eastern sector **(Figure. 4.3.4.)** with a maximum located slightly to the east of the wind speed maximum. Positive correlation extends southwards to -10°S although it has a small correlation; it is still significant at the 95% confidence level. Negative correlations can be observed in the Mediterranean and the Labrador Sea.

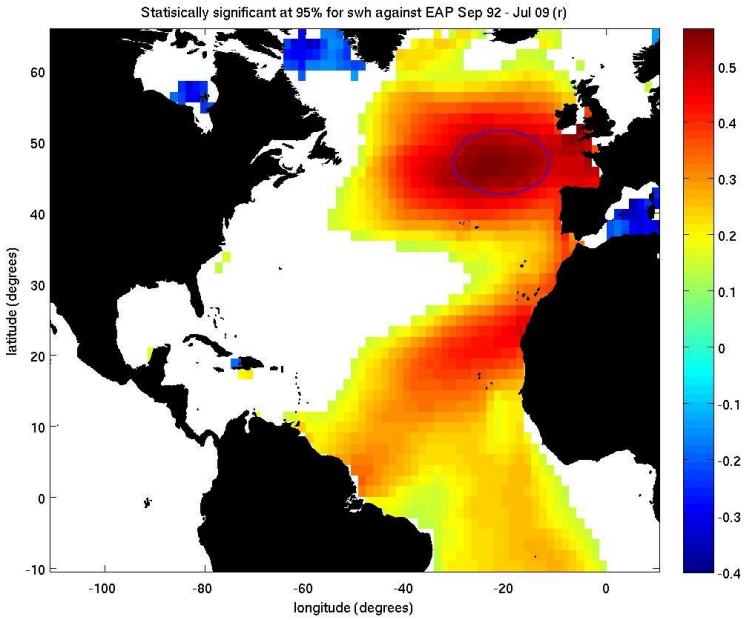

Figure. 4.3.4. 95% Confidence level of swh anomalies against EAP anomalies from ERA-Interim September 1992 – July 2009

4.3.3. Altimeter swh

Results from the EOF analysis of the swh satellite data shows the e2-n1 data is more influenced by the atmospheric modes so I will compare this against the model data. The correlations against the NAO (**Figure. 4.3.5.**) shows the model data is fairly accurate; however the satellite data gives somewhat lower correlation.

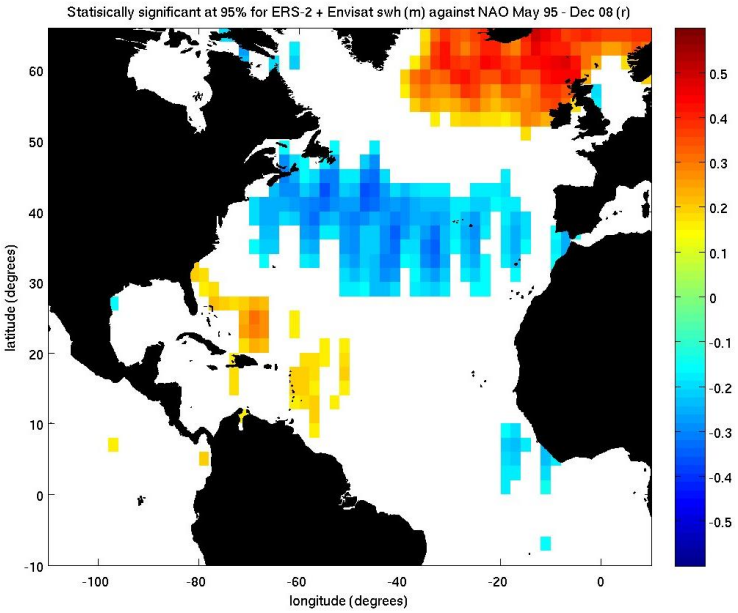

Figure. 4.3.5. 95% Confidence level of swh anomalies against NAO anomalies from ERS-2 + Envisat May 1995 – December 2008

Correlation against the EAP is shown in **Figure. 4.3.6.** The correlation of the satellite data is less in magnitude. It shows less correlation in the south but extends slightly into the Pacific. The coherence of the negatively correlated area decreases.

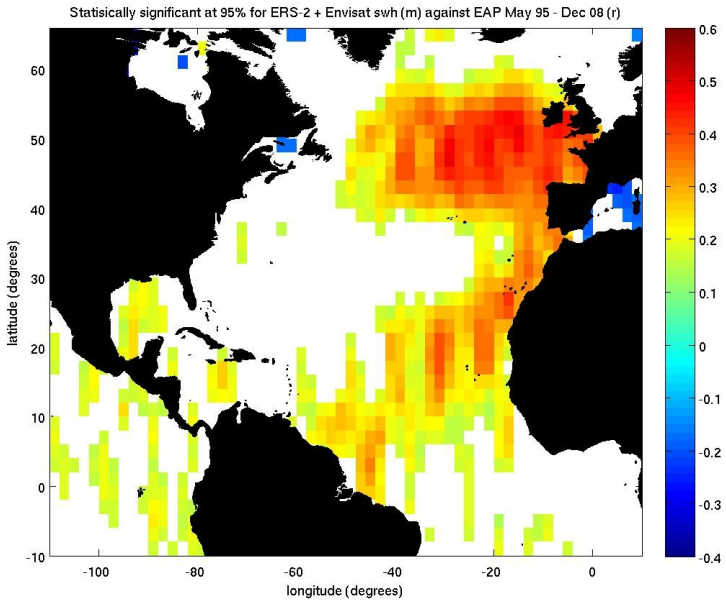

Figure. 4.3.6. 95**%** Confidence level of swh anomalies against EAP anomalies from ERS-2 + Envisat May 1995 – December 2008

The maximum correlation of swh against the climate indices is slightly to the right of where the wind speed shows maximum correlation. This is expected as the magnitude of swh depends on the local wind speed and swell waves associated with distant storms (Trigo *et al*, 2008). Trigo *et al* (2008) used the winter months of swh from the C-ERA-40 dataset (Sterl and Caires *et al*, 2005), which gives a larger swh, and obtained a similar spatial correlation against the NAO, however he obtained stronger correlations, likely to be due to the winter months or the slightly different wave field given from C-ERA-40. There are large changes in comparison to his EAP correlation. The positive area expands in size and the negative correlation to the north of the British Isles disappears in my study, possibly as the EAP has gone into a more prolonged positive phase in recent years. Unfortunately his study only uses a region of 20°N-75°N, 75°W-20°E, so comparisons in the south and west of my plot cannot be made. Lionello and Galati (2008) observed the correlation of five different atmospheric modes in the Mediterranean. His results also shows the NAO and EAP give a negative correlation of similar magnitude in the western Mediterranean. The di-pole in the north east region of the plot has previously been studied (Cotton and Challenor, 1999; Woolf *et al*, 2002) however there is also another band of positive correlation located in the western tropical Atlantic. Similar to the wind speed the NAO has a profound effect on the swh in the North Atlantic yet the EAP has a stronger positive correlation coherence with smaller areas of negative correlation.

4.3.4. ERA mwp

The NAO has a strong influence on mwp across most of the North Atlantic (**Figure. 4.3.7.**). It is maximally correlated to the north west of the British Isles with **r = 0.6** and it has a minimum correlation in most of the mid Atlantic which extends to the south with **r = -0.4**. A

dividing line is clear from the tip of Greenland down to North West Africa which separates the correlations. An area of small positive correlation is present in the west, similar to swh.

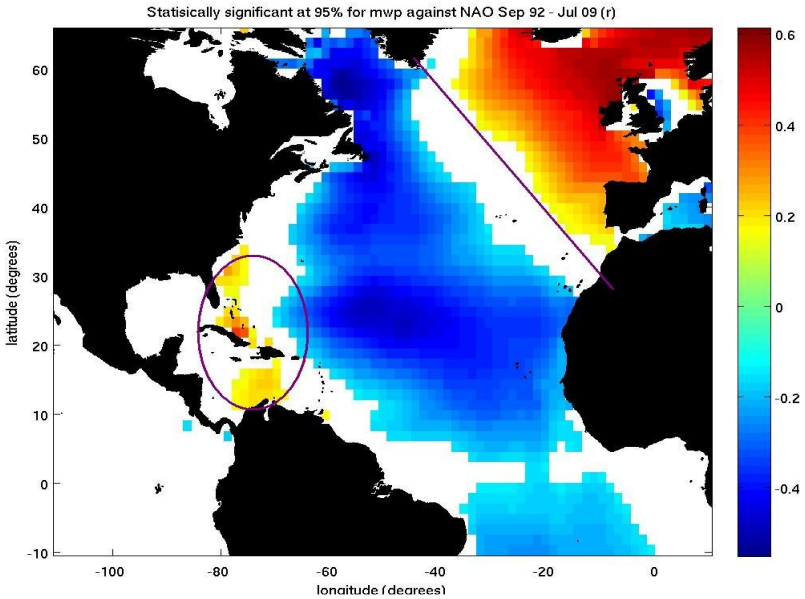

Figure. 4.3.7. 95**%** Confidence level of mwp anomalies against NAO anomalies from ERA-Interim September 1992 – July 2009

The correlation of EAP against the mwp shows a maximum around the Bay of Biscay (**Figure. 4.3.8.**) with **r = 0.5**. There is also negative correlation in the North Sea of **r = -0.3**, otherwise, the plot is similar to swh against EAP.

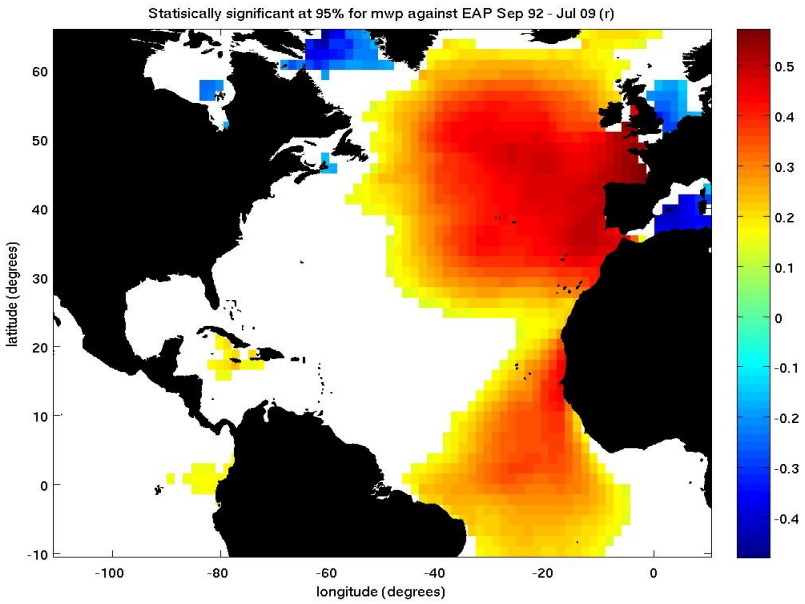

Figure. 4.3.8. 95**%** Confidence level of mwp anomalies against EAP anomalies from ERA-Interim September 1992 – July 2009

4.3.5. Altimeter T_z

The strongest relation between T_z and atmospheric modes of the satellite data came from tx-j1. Therefore I have used this as a comparison to the model data. The area of correlation with the NAO is greatly reduced and more north east – south west alternative bands emerge (**Figure. 4.3.9.**).

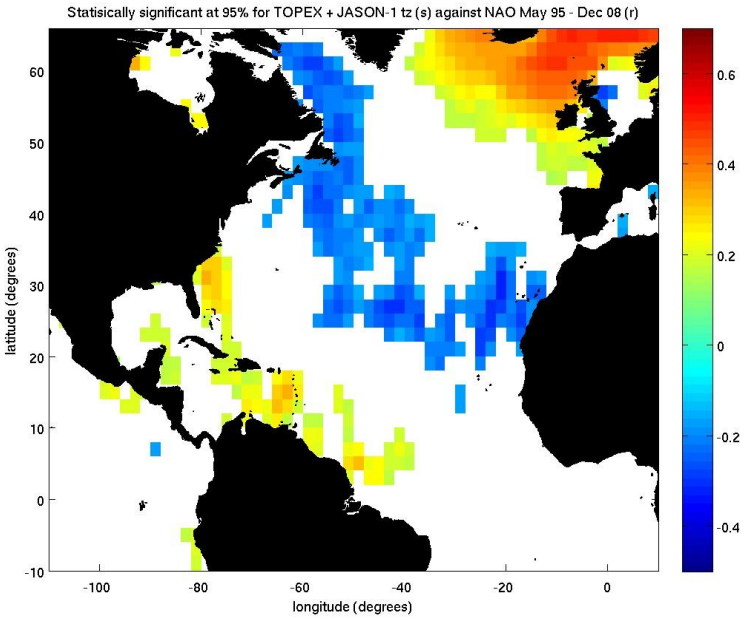

Figure. 4.3.9. 95**%** Confidence level of T_z anomalies against NAO anomalies from TOPEX + Jason-1 May 1995 – December 2008

The correlation against the EAP shows the positive correlation coherence decreases and its magnitude also slightly decreases (**Figure. 4.3.10.**). The negatively correlated areas are fairly similar apart from a slight decrease in the Labrador Sea.

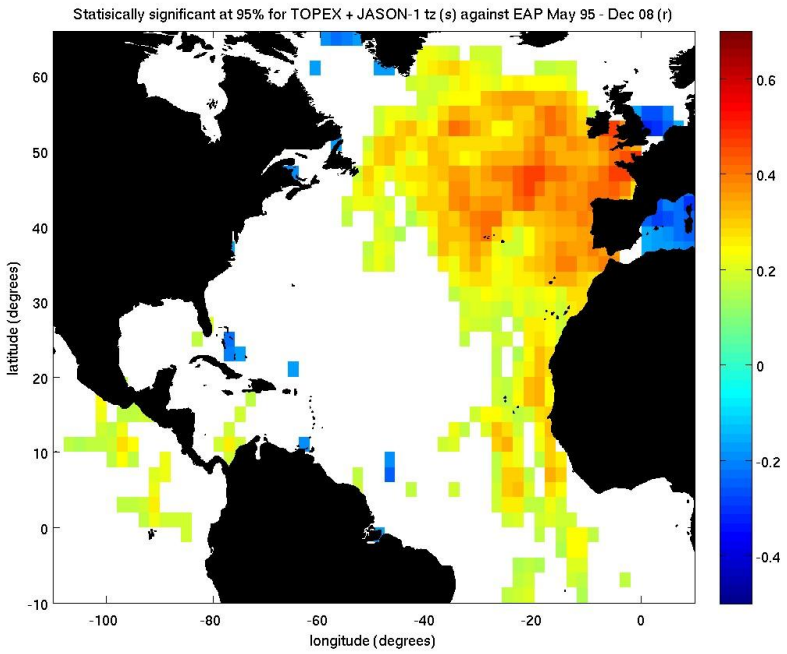

Figure. 4.3.10. 95**%** Confidence level of T_z anomalies against NAO anomalies from TOPEX + Jason-1 May 1995 – December 2008

There have been no other studies investigating wave period anomalies against climate index anomalies. The results against the EAP are similar with swh, but the correlation against the NAO shows some minor differences. The NAO influences the wave period by means of more north west – south east alternate bands as opposed to zonal bands observed in the wind speed and swh. This is also true for the spatial maps of the EOFs which are most correlated with the NAO.

4.4. Spatial correlation with lagged MEI

4.4.1. wind speed

The lagged time series of wind speed anomalies from ERA-Interim against the MEI anomalies is shown in **wind_MEI_space_lag_95.mov**. A lag of 3 months shows 3 alternate bands emerge in the Atlantic. A positive correlated area emerges to the northeast of Brazil

with **r = 0.3**. A negatively correlated area of **r = 0.2-0.3** in the eastern Atlantic and a small positively correlated area at 30°N, 60°W, with a small magnitude of **r = 0.2**. The positive correlation area on the Equator moves eastward towards Africa up to 15 months after. After 18 months a small patch at 30°N, 30°W, has a positive correlation of **r = 0.35**. This small patch moves north eastwards until 25 months after. Following a lag of 25 months the data becomes spurious. After 42 months there is a small band of positive correlation at 20°N, 20°W, negatively correlated area in the west at 30°N and a small area of positive correlation to the west of the British Isles.

It has previously been found that wind speed in the tropical North Atlantic is related to wind speeds from certain areas in the tropical Pacific (Enfield and Mayer, 1997; Klein *et al*, 1999). During El Niño events wind speed decreases in the tropical North Atlantic as anomalous south-westerlies oppose the mean trade wind easterlies. However, other studies show in strong El Niño events the North Atlantic amplifies the wind speed signal of the Pacific with a lag of approximately 3-5 months, between 5-22.5°N, 60°W-18.5°W (Bell, 2009). I concur with these results especially in the west tropical North Atlantic. I find amplifications of wind speeds after approximately a 5 month lag but only a small area which is 95% statistically significant in the west. The area of positive correlation which spreads east from the Caribbean Sea is also present in other studies as this region is associated with westerly winds bursts (Shaw, 2008; Lee *et al*, 2008). It takes approximately 2 years for El Niño events to affect regions in close proximity to the Gulf stream (Taylor, 1998) as the anomalous signal either travels to the tropical Atlantic and then to Ferrell cell by meridional transport in the Hadley cell or travels to the Hadley cell in the Pacific and then across to the North Atlantic by planetary stationary waves.

To understand further teleconnections of ENSO in the North Atlantic it should be noted ENSO can influence atmospheric modes such as the NAO. The sea level pressure anomaly

pattern has been related to a positive NAO phase during the winter, following autumns of strong La Niña's (Pozo-Vazquez *et al*, 2005). Similarly, mean sea level pressure correlation shows ENSO can act to push the NAO into a negative state by raising pressure near the Icelandic low and decreasing pressure near the Azores high (Shaw, 2008). However, these types of signals cannot be identified with my data.

4.4.2. swh

The lagged swh time series from ERA-Interim shows that there are significant areas likely to be affected by teleconnection processes from the tropical Pacific (**swh_MEI_space_lag_95.mov**). An area of strong negative correlation initially occurs in the west tropical North Atlantic. This area is not statistically significant at the 95% in the wind speed and therefore should be observed with care as the swell waves are likely to be small here as well. A maximum positive correlation occurs in the Bahamas of **r = 0.3** after a lag of 4 months, this is similar to the wind speed. After 21 months a large positively correlated area at 30°N, 30°W, emerges with **r = ~0.28** which travels north east from a lag of 15 months to 23 months. This is also present in the wind speed (**wind_MEI_space_lag_95.mov**). After 42 months a large patch of negative correlated area with **r = -0.3** at 30°N, 40°W. This is not prominent in the wind speed.

To complement the model's homogenous spatial data I studied the correlation of MEI with swh from the more accurate e2-n1 (**e2_n1_swh_MEI_space_lag_95.mov**). The data does not show the strong negative correlation at month 0 in the tropical West Atlantic unlike the model data. The positive correlation in the Caribbean Sea is present with a similar magnitude. The positive correlation is also present after 19 months in the east central North Atlantic but is less coherent, due to the altimeters trackiness.

There have been no studies investigating ENSO's influence on the wave field in the North Atlantic. The probable teleconnections of swh with the MEI are likely to be similar to the areas which are present in the correlations of the wind speed. However, the correlation may not be statically significant at 95% in the wind speed but is in the swh, as swh is also influenced by swell waves, therefore does not give clear links.

4.4.3. wave period

The lagged MEI against the mwp from ERA-Interim is shown in **mwp_MEI_space_lag_95.mov**. A patch shows strong positive correlation in the Bahamas slightly to the west of the maximum located in swh after 6 months with **r = 0.2**. A small area in the western Atlantic with a positive correlation of **r = 0.25-3** occurs after 27 months. After 42 months a huge area in the western Atlantic is negatively correlated to MEI of **r = 0.3** also in swh (**swh_MEI_space_lag_95.mov**).

To also complement this model data I studied the correlation of a lagged MEI with the more accurate tx-j1 T_z. (**tx_j1_tz_MEI_space_lag_95.mov**). The positive correlation in the Caribbean Sea is also present after 6 months. A large area with positive correlation is located in south with **r = ~0.3** after 20 months which is not observed in the wind speed or swh correlations whereas the area with positive correlation after 27 months is not present. There is only a small area in the central region with negative correlation of **r = 0.2.** after 42 months.

The influence of the ENSO on wave period in the North Atlantic is not obvious from this data. The results for mwp from the model may not hold with the same correlations of swh and wind speed. The atmospheric mode of the NAO influences swh in a slightly different way to wave period. However, the EAP influences swh and wave period similarly. It is likely that ENSO has an observable positive influence of the wave field in the western tropical North

Atlantic after approximately 6 months and the central North Atlantic after approximately 20 months.

5. Conclusion

A first comparison of ERA-40 and ERA-Interim revealed differences between wind speed, swh and wave period. The differences in swh and wave period were evaluated further in comparison to the satellite data.

Wind speed:

- This is the most similar parameter between the two models. ERA-Interim provides a marginally greater maximum wind speed than ERA-40, which is more accurate; however it is still underestimated in comparison to previous calibrated altimeter results.

- There are small changes in the EOF analysis between ERA-40 and ERA-Interim. The first and second modes are slightly more correlated to the NAO than the EAP.

Significant wave height:

- ERA-Interim gives larger maximum swh than ERA-40, which are more correct. However, the maximum ERA-Interim swh is underestimated compared to the satellite altimeter data. The underestimated wind speeds in ERA-Interim are likely to have caused the underestimated swh in comparison to the satellite altimeter results. The increased resolution in ERA-Interim would allow for storms to be better resolved and therefore likely to be one of the main causes for an increased swh in comparison to ERA-40. In addition, the WAM has been improved in ERA-Interim.

- The time inhomogeneities have been reduced in ERA-Interim compared to ERA-40, especially in the earlier 1990s.

- There are small differences in the EOF analysis from the model data of ERA-40 and ERA-Interim. The EOF analysis of satellite data shows a reduction of the first and second modes in comparison to ERA-Interim by approximately 10% and 7%, respectively.

- The longer time series satellite data showed EOF 1 had a much stronger correlation with the EAP and EOF 2 has a much stronger correlation with the NAO but a greater magnitude, in comparison to the shorter time period of satellite data.

- The difference in swh obtained from 10 day repeat cycle and 35 day repeat cycle altimeter datasets are fairly small, with minor discrepancies in different months.

Wave period:

- The wave periods are not directly comparable as the model uses mwp (T_e) and the altimeters T_z.

- The maximum mwp for both models are much larger than the altimeter data and previous studies of ERA-40 mwp. ERA-Interim gives slightly lower maximum mwp results but both models are still not very accurate compared to the satellite data. The larger mwp results may have come from the free ERA-40 and ERA-Interim online dataset in comparison to the complete ERA-40 and ERA-Interim datasets available to paid ECMWF users which have greater spatial and temporal resolution and are used in academic studies. Alternatively, there may have been an error on the ECMWF

website (http://www.ecmwf.int/research/era/do/get/index) on the date when the data was downloaded or simply a personal error in data processing.

- Large differences are observed in the EOFs of ERA-40 and ERA-Interim. The first EOF in ERA-Interim decreases to 27% from explaining 47% of the variance obtained with ERA-40 and has a slightly different spatial pattern. It is only at EOF 3 that the model data shows expected forcing from the atmospheric modes. Both models give inaccurate spatial results compared to the altimeters. tx-j1 has the first two EOFs linked to atmospherics modes.

- The differences in T_z from the 10 day and 35 day repeat cycle altimeter datasets are noticeable, as tx-j1 gives larger values for most months in comparison to e2-n1.

- There are large differences in the EOF analysis between the 10 day and 35 day repeat cycle altimeter datasets. e2-n1 gives a much larger first mode at 39% where as tx-j1 explains 16.3% of the variability. The ERS-2 data was shown to give negative T_z which had to be excluded. Further analysis is required to ascertain if large differences are found in Envisat as well when compared to TOPEX and Jason-1.

- The most accurate dataset is likely to be tx-j1 as the first EOF corresponds to the EAP and the second EOF corresponds to the NAO, with the largest magnitude.

- The NAO's influence on EOF 1 has also decreased recently for wave period from 1993-2002 compared to 1995-2008 and the EAP's influence on EOF 1 has slightly increased.

During winter months the wind speed, swh and mwp were shown to display a significant inter-annual variability, illustrated by standard deviations of the order 1.5 m/s, 1m and 1s, respectively for the full ERA-Interim dataset used from September 1992 – July 2009.

The spatial patterns caused by the atmospheric modes are understood further with correlations of parameter anomalies against climate index anomalies:

- The EAP is observed to give a larger positive coherent spatial pattern.
- The NAO gives a stronger magnitude of positive correlation but shows larger areas of negative correlation in the central Atlantic.

Only recently have studies shown the EAP can almost have as much influence on the location of storm tracks as the NAO (Seierstad *et al*, 2007) as well as other parameters (Lionello and Galati *et al*, 2008). Further work is required to study if the change in regime in the NAO and EAP is present in the winter months.

The study of MEI anomalies regressed against parameter anomalies in the North Atlantic revealed:

- Wind speed teleconnections in the western tropical Atlantic, as the MEI increases wind speed with a maximum magnitude after approximately 6 months. In addition, an area in the central Atlantic shows a positive correlation with the MEI with a maximum after approximately 20 months.
- These teleconnections have a similar effect on swh and wave period.

It would be interesting to study extreme events such as the strong El Niño of 1998 (McPhaden, 1999) and follow its teleconnections in the North Atlantic as well as the strong La Niña of 1999. Further work with the EOFs are required to observe if these teleconnection patterns explain any variability in the North Atlantic by extending the number of EOFs studied and lagging the respective PC against the MEI and focussing in the tropical Western Atlantic.

The World Meteorological Organization (WMO) recommends climate to be based on 30 years worth of data (Sterl and Caires, 2005). A few more years are required to be able to accurately quantify interdecadal variability using altimeters, similarly with the new ECMWF re-analysis product ERA-Interim.

- The wave climate has become calmer in the longer period study from 1992 - 2009 compared to 1992-2002, possibly as the 1990s had the greatest global swh results on record from ERA-40 - 1992, 1993 and 1994 (Sterl and Caires, 2005).

Further study is required to compare the results from the 2000s to the 1990s to investigate recent interdecadal variability. Other studies do show an increase in swh trends since the 1950s (Sterl and Caires, 2005; Gulev and Grigorieva, 2006; Dodet *et al*, 2010), likely due to the northwards shift of storm tracks (Trenberth *et al*, 2007).

The limitations of the re-analysis models in this data have been identified using altimeters; however, the altimeters are not without their limitations. Rain cells in clouds can affect the attenuation of pulses and cause erroneous data. Also, altimeters cannot measure ocean parameters if the footprint overlaps land, so other processes are required to obtain coastal

information (Robinson, 2004). The altimeter data shows trackiness set by the narrow footprint as the individual passes are separated in time. This can be improved with merged satellite data products and calibration against buoy data (Queffeulou and Bentamy, 2007; Cromwell and Gommenginger, 2009). Current work is being undertaken at the National Oceanography Centre Southampton to use Optimal Interpolation methods to reduce the trackiness observed. Recently there has been a surge in SAR measurements of the wave climate which have greater spatial resolution and can measure wave direction, also given by the re-analysis models (Schulz-Stellenfleth *et al*, 2007; Li *et al*, 2008; Lehner *et al*, 2009), however climatology studies are non-existent.

This study shows the need for a concurrent use of wave models and satellite measurements to mitigate their respective limitations.

Future work with these observations should be investigated such as:

- Removing the Great Lakes from the analysis to remove most of the spurious data from both the model and the altimeters and increase the correlations.
- Investigate sub regions in the North Atlantic to increase the correlation with the climate indices such as the north east region especially by studying the winter months.
- The western tropical Atlantic is shown to show links with the NAO and MEI and further analysis is required to observe in which season the teleconnections are strongest.
- Investigate the extent of influence form other atmosphere modes such as the Scandinavian Pattern and East Atlantic/West Russian pattern on the North Atlantic's wave field (Lionello and Galati, 2008).

- The techniques in this study can be applied to other basins such as the Pacific and its influence from the various NINO regions on the wind and wave climate.

References

Alexander, M.A., Blade, I., Newman, M., Lanzante, J.R., Lau, N. and Scott, J.D. (2002) The atmospheric bridge: The influence of ENSO teleconnections on Air-Sea interaction over the global oceans. *Journal of climate.* **15.** pp. 2205-2231.

Andersson, E., Haseler, J., Und´en, P., Courtier, P., Kelly, G., Vasiljevic, D., Brancovic, C., Cardinali, C., Gaffard, C., Hollingsworth, A., Jakob, C., Janssen, P., Klinker, E., Lanzinger, A., Miller, M., Rabier, F., Simmons, A., Strauss, B., Th´epaut, J.-N. and Viterbo, P. (1998) The ECMWF implementation of three-dimensional variational assimilation (3D-Var). III: Experimental results. *Quarterly Journal of the Royal Meteorological Society*, **124,** pp. 1831–1860.

Bacon, S. and Carter, D. J. T. (1991) Wave climate changes in the North Atlantic and North Sea, *International Journal of Climatology*, **11**, pp. 545 – 558.

Barnston, A.G., and Livezey, R.E. (1987) Classification, seasonality and persistence of low - frequency atmospheric circulation patterns. *Monthly Weather Review*, **115**, pp. 1083-1126.

Barrick, D. E., (1974) Wind dependence of quasi-specular microwave sea scatter, *IEEE Transactions on Antennas and Propagation*., **AP-22**, pp. 135– 136.

Bauer, E. and Staabs, C. (1998) Statistical properties of global significant wave heights and their use for validation. *Journal of Geophysical Research*, **103**, pp. 1153–1166.

Bauer, E., and Weisse, R. (2000) Determination of high-frequency wind variability from observations and application to North Atlantic wave modeling, *Journal of Geophysical Research*, **105(C11)**, pp. 26,179– 26,190.

Baxevani, A., Borgel, C. and Rychlik, I. (2007) Spatial modes for the variability of the significant wave height on the worlds ocean. *Proceedings of the Sixteenth International Offshore and Polar Engineering Conference. Lisbon, Portugal, July 1-6, 2007.*

Bidlot, J.-R., Janseen, P.A.E.M., Abdalla, S. and Hersbach, H. (2007) A revised formulation of ocean wave dissipation and its model impact, *ECMWF Technical Report Memorandum, 509.* European Centre for Medium-Range Weather Forecasting, Reading, UK.

Bell, R.J. (2009). *The influence winds have on SST and SSHa in the tropical Pacific – The 1997/1998 El Niño*, University of Southampton undergraduate project. P.31. Unpublished manuscript.

Berrisford, P., Dee, D., Fielding, K., Fuentes, M., Kållberg, K., Kobayashi, S., Uppala, S., (2009). ECMWF ERA report series: 1. The ERA-interim archive. Version. 1. pp. 20.

Burgerson, G. and Stephenson, D.B. (1998) The normality of El Niño. *Geophysical Research Letters.* **8(26)**. pp. 1027-1030.

Caires, S. and Sterl A. (2003) Validation of ocean wind and wave data using triple collocation. *Journal of Geophysical Research*, **108**, **3098**

Caires, S. and Swail, V. (2004) Global wave climate trend and variability analysis. *8th International workshop on wave hindcasting and forecasting*. North Shore, Oahu, Hawaii, 14-19 November

Caires, S., Sterl, A. Bidlot, J. R. Graham, N. and Swail V. R. (2004) Intercomparison of different wind wave reanalysis. *Journal of Climate*, **17**, pp. 1893–1913.

Caires, S., Sterl, A. and Gommemginger, C.P. (2005) Global ocean mean wave period data: validation and description, *Journal of Geophysical Research*., **110, C02003**

Cavaleri, L. The WISE Group., Alves, J-H.G.M., Ardhuin, F., Babanin, A., Banner, M., Belibassakis, K., Benoit, M., Donelan, M., Groeneweg, J., Herbers, T.H.C., Hwang, P., Janssen, P.A.E.M., Janssen, T., Lavrenov, I.V., Magne, R., Monbaliu, J. Onorato, M., Polnikov, V., Resio, D., Rogers, W.E., Sheremet, A., McKee Smith, J., Tolman, H.L., Vledder, G.van., Wolf, J. and Young, I. (2007). Wave modelling – The state of the art. *Progress in Oceanography*. **75,** pp.603-674.

Chang, E.K.M., Lee, S. and Swanson, K.L. (2002) Storm track dynamics, *Journal of Climate*, **15**, pp. 2163– 2183.

Chen, G.E., Bi, W.S. and Ma, J. (2003) Global structure of marine wind speed variability derived from TOPEX altimeter data. *International Journal of Remote Sensing*. **24(24)**, pp. 5119-5133.

Chen, G.E., Ezraty, R., Fang, C. And Fang, L. (2002) A new look at the zonal pattern of the marine wind system from TOPEX measurements. *Remote Sensing of Environment.* **79.** pp. 15-22.

Cheng, C-L. and Van Ness, J.W. (1999) *Statistical regression with measurement error*, p. 262.

Cotton, P.D., Challenor, P.G. and Carter, D.J.T. (1997) Variability altimeter global wave climate data. *In. ''Ocean Wave Measurements and analysis: Preoceedings of the third international symposium WAVES '97''* pp. 819-826. Nov 3-7, Virginia Beach, VA.

Cotton, P.D. and Challenor, P.G. (1999) North Atlantic wave climate variability and the North Atlantic Oscillation index, in ‘‘*proc. 9th international offshore and polar engineering conference*’’ Brest, France, III pp.153-157.

Cromwell, D. and Gommenginger, C. (2009) Developing global long-term altimeter datasets and climatologies of ocean wave measurements, *OceanObs 2009 21-25 September, Venice, Italy*

Davies, G.C., Challenor, P.G., and Cotton, P.D. (1998) Measurements of wave period from radar altimeters. in ‘‘Ocean wave measurement and analysis: proceedings of the third international symposium WAVES ’97,’’ pp. 819-826. Nov. 3-7, Virginia Beach, VA.

Dee, D. and Uppala, S. (2008) Variational bias correction in ERA-Interim. *ECMWF Tech. Rep. Memorandum*. October 2008.

Dodet, G., Bertin, X. and Taborda, R. (2010) Wave climate variability in the North-East Atlantic Ocean over the last six decades. *Ocean Modelling.* ***31.*** pp. 120-131.

Dommenget, D., and Latif, M., (2002) A cautionary note on the interpretation of EOFs. *Journal of Climate*. **15(2)**. pp. 216-225.

Dupuis, H., Denis, M., and Aldo, S. (2006) Wave climate evolution in the Bay of Biscay over two decades**.** *Journal of Marine Systems* **63(3-4)** pp. 105-114.

Emery, W.J. and Thomson, R.E. (2001) *Data analysis methods in physical oceanography*. P. 634.

Enfield, D.B., and Mayer, D.A. (1997) Tropical Atlantic sea surface temperature variability and its relation to El Niño-Southern Oscillation. *Journal of Geophysical Research.* **102.** pp. 929-945.

Fu, L. and Cazenave, A. (2001) *Satellite altimetry and earth sciences: A handbook of techniques and applications*. P. 463.

Golden Gate Weather Services (2000) ENSO glossary. Available online from: [http://ggweather.com/enso/nino_regions.gif]. Accessed 27th March 2009.’

Gommenginger, C.P., Srokosz, M.A., Challenor, P.G. and Cotton, P.D. (2003) Measuring ocean wave period with satellite altimeters: A simple empirical model, *Geophysical Research Letters*, **30(22)**, pp. 2150-2155.

Greenslade, D.J.M. and Young, I.R. (2004) Background errors in a global wave model determined from altimeter data. *Journal of Geophysical Research.* **109,C09007.**

Greenslade, D.J.M. and Young, I.R. (2005) The Impact of Altimeter Sampling Patterns on Estimates of Background Errors in a Global Wave Model. *Journal of Atmospheric and Oceanic Technology.* **22.** pp. 1895-1917.

Grevemeyer, I., Herber, R. and Essen,H-H., (2000) Microseismological evidence for a changing wave climate in the northeast Atlantic Ocean, *Nature*, **408**, pp. 349– 352.

Günther, H., Rosenthal, W., Stawarz, M., Carretero, J.C., Gomez, M., Lozano, I., Serano, O. and Reistad, M. (1998) The wave climate of the Northeast Atlantic over the period 1955-94: the WASA wave hindcast. *Global Atmosphere and Ocean System*, **6**, pp. 121-163.

Gulev, S.K. and Grigorieva, V. (2006) Variability of the Winter Wind Waves and Swell in the North Atlantic and North Pacific as Revealed by the Voluntary Observing Ship Data. *Journal of Climate.* **19.** pp. 5667-5685.

Gulev, S.K., Cotton, I.D. and Sterl, A. (1998) Intercomparison of the North Atlantic Wave Climatology from Voluntary Observing Ships, Satellite Data and Modelling. *Physics and Chemistry of the Earth*, **23(5-6**), pp. 587 592.

Hurrell, J. W. (1995) Decadal trends in the North Atlantic Oscillation: regional temperatures and precipitation, *Science*, **269**, pp. 676-679.

Hurrell, J. W., and Deser, C. (2009) North Atlantic climate variability: The role of the North Atlantic Oscillation. *Journal of Marine Systems*, **78(1),** pp. 28-41

Hurrell, J. W., and Van Loon, H. (1997) Decadal variations in climate associated with the North Atlantic Oscillation, *Climatic Change*, **36**, pp. 301-326.

Hwang, P.A., Teague, W.J., Jacobs, G.A. and Wand, D.W. (1998) A statistical comparison of wind speed, wave height and wave period derived from satellite altimeters and ocean buoys in the Gulf of Mexico. *Journal of Geophysical Research.* **103**. pp.10451-10468.

Janssen, P.A.E.M., Doyle, J.D. Bidlot, J. Hansen, B. Isaksen, L. and Viterbo, P. (2002) Impact and feedback of ocean waves on the atmosphere, *in Advances in Fluid Mechanics*, **vol. 1**, edited by W. Perrie, pp. 155–197, WIT Press, Southampton, England,

Jones, P. D., Osborn, T.J. and Briffa, K.R. (2003) Pressure-based measurements of the North Atlantic Oscillation (NAO): A comparison and an assessment of changes in the strength of the NAO and in its influence on surface climate parameters, in The North Atlantic Oscillation: Climatic Significance and Environmental Impact, *Geophysical. Monograph. Series*., **134**, edited by J. W. Hurrell *et al*., pp. 51– 62, AGU, Washington, D. C.

Josey, S.A. and Marsh, R. (2005) Surface freshwater flux variability and recent freshening of the North Atlantic in the eastern subpolar gyre, *Journal of Geophysical Research*, **110**, **C05008**

Klein, S.A., Soden, B.J. and Lau, N.C. (1999) Remote sea surface variations during ENSO: Evidence for a tropical atmospheric bridge. *Journal of climate,* **12(4)**, pp. 917–932.

Komen G.J., Cavaleri, L., Donelan, M., Hasselmann, K., Hasselmann, S., Janssen, P.A.E.M. (1994) *Dynamics and Modelling of Ocean Waves,* p.532

Kushnir, Y., Cardone, V.J., Greenwood, J.G. and Cane, M.A. (1997) The recent increase in North Atlantic wave heights, *Journal of Climate*, **10(8),** pp. 2107–2113,

Krogstad, H.E., and Barstow, S.F. (1999) Satellite wave measurements for coastal engineering applications, *Coastal Engineering*, **37(3-4),** Pp. 283-307.

Lee, S.-K., Enfield, D.B. and Wang, C. (2008) Why do some El Niño's have no impact on tropical North Atlantic SST? *Geophysical Research Letters.*, **35**, **L16705**.

Lehner, S., Li, X.M., and Brusch, S. (2009) Global ENVISAT ASAR and coastal TerraSAR X Measurements of Sea State for validation of Ocean Wave Models. *11th Wave Workshop*. Halifax, Canada, October 18th-23th.

Li, X. M., Lehner, S. and He, M.X. (2008) Ocean wave measurements based on satellite synthetic aperture radar (SAR) and numerical wave model (WAM) data - extreme sea state and cross sea analysis, *international Journal of Remote Sensing* . **29(21)**, pp. 6403-6416.

Lionello, P. and Galati, M.B. (2008) Links of the significant wave height distribution in the Mediterranean sea with the North Hemisphere teleconnections patterns. *Advances in Geosciences.* **17.** pp. 13-18.

Liu, Z. and Alexander, M. (2007) Atmospheric bridge, oceanic tunnel, and global climatic teleconnections. *Review of Geophysics.* **45. RG2005**

Mackay, E.B.L., Bahaj, A.S. and Challenor, P.G. (2010) Uncertainty in wave energy resource assessment. Part 2: Variability and predictability. *Renewable energy,* **35(8).** pp. 1809-1819.

Mackay, E.B.L., Retzler, C.H., Challenor, P.G., and Gommenginger, C. P. (2008) A parametric ocean model for wave period from K_u band altimeter data. *Journal of Geophysical Research* **113(C03029)**.

Marshall, J., Kushnir, Y., Battisti, D., Change, P., Czaja, A., Dickson, R., Hurrell, J., McCartney, M., Saravanan, R. and Visbeck, M. (2001) North Atlantic climate variability: Phenomena, impacts and mechanisms. *International Journal of Climatology* , **21(15)**, pp. 1863-1898.

McPhaden, M.J. (1999) Genesis and evolution of the 1997-98 El Niño. *Science*. **283(5404).** pp. 950-954

McPhaden, M.J. (2000) TAO diagrams. Available online from: [http://www.pmel.noaa.gov/tao/proj_over/diagrams/index.html]. Accessed 2nd March 2009.

NOAA CPC (2008) East Atlantic. Available online from: [http://www.cpc.noaa.gov/data/teledoc/ea.shtml]. Accessed 24th April 2010.

Osborn, T.J. (2006) Recent variations in the winter North Atlantic Oscillation. *Weather* **61**, pp. 353-355.

Pozo-Vazquez, D., Gámiz-Fortis, S.R., Tovar-Pescador, J., Esteban-Parra, M. J. and Castro-DÍez, Y. (2005) North Atlantic SLP anomalies based on the Autumn ENSO State**.** *Journal of Climate*, **18(1)**, pp. 97-103.

Preisendorfer, R.W. (1988) *Principal component analysis in meteorology and oceanography*. p. 425.

Queffeulou, P. and Bentamy, A. (2007) Analysis of Wave Height Variability Using Altimeter Measurements: Applications to the Mediterranean Sea. *Journal of Atmospheric and Oceanic Technology,* **24.** pp. 2078-2092.

Quilfen, Y., Chapron, B. and Serre, M. (2004) Calibration/validation of an altimeter wave period model and application to TOPEX/Poseidon and Jason-1 altimeters, *Marine Geodesy*., **27**, pp. 535– 549.

Rabier, F., Järvinen, H., Klinker, E., Mahfouf, J.F. and Simmons, A.J. (2000) The ECMWF operational implementation of four-dimensional variational assimilation. I: Experimental results with simplified physics. *Quarterly Journal of the Royal Meteorological Society*, **126,** pp. 1143–1170

Robinson, I.R. (2004) *Measuring the oceans from space: The principles and methods of satellite oceanography*. P. 669.

Rogers, J.C. (1997) North Atlantic storm track variability and its association to the North Atlantic Oscillation and Climate Variability of Northern Europe. *Journal of Climate*, **10**, pp. 1635-1647.

Sasaki, W. and Hibiya, T. (2007) Interannual Variability and Predictability of Summer time Significant Wave Heights in the Western North Pacific. *Journal of Oceanography*, **63**, pp. 203 - 213.

Schulz-Stellenfleth, J., Konig, T. and Lehner, S. (2007) An empirical approach for the retrieval of integral ocean wave parameters from synthetic aperture radar data, *Journal of Geophysical Research*., **112, C03019**,

Seierstad, I.A., Stephenson, D.B. and Kvamstø, N.G. (2007) How useful are teleconnection patterns for explaining variability in extratropical storminess, *Tellus*, **59A,** pp. 170-181.

Semedo, A. and Sušelj, K., Rutgersson, A. and Sterl, A. (2009) A global view of the wind sea and swell waves interannual variability from ERA-40. p. 20 (Submitted to Journal of Climate)

Shaw, B. (2008) ENSO teleconnections and the North Atlantic Ocean. An exercise in correlation. MPO 672 – ENSO Dynamics, Prediction and Predictability. p. 7.

Simmons, A. J. and Hollingsworth, A. (2002) Some aspects of the improvement in skill of numerical weather prediction. *Quarterly Journal of the Royal Meteorological Society*, **128,** pp**.** 647–677

Simmons, A., Uppala, S., Dee, D. and Kobayashi, S. (2007) *ERA-Interim: New ECMWF reanalysis products from 1989 onwards.* **Newsletter 110** - Winter 2006/07, ECMWF, 11 pp

Sterl, A. and Caires, S. (2005) Climatology, variability and extreme of ocean waves: The web based KNMI/ERA-40 wave atlas. *International Journal of Climatology*. **25(7).** pp. 963-977. Full edition Available online [http://www.knmi.nl/onderzk/oceano/waves/era40/license.cgi] accessed 16th February 2010.

Sterl, A., Komen, G.J., and Cotton, P.D. (1998) Fifteen years of global wave hindcasts winds from the European centre for medium range weather forecasts reanalysis: validating the reanalyszes winds and assessing the wave climate. *Journal of Geophysical Research* **103.** pp. 5477-5492.

Storch, H.V. and Francis, W.Z. (2001) *Statistical analysis in climate research*. p. 484.

Sykes, N. (2005) *Changes in wind and wave climate observed from space*. MSc project. University of Southampton. p. 58.

Taguchi, M. and Hartmann, D.L. (2005) Interference of extratropical surface climate anomalies induced by El Niño and stratospheric sudden warmings, *Geophysical Research. Letters*., **32, L04709**,

Taylor, A.H., Jordan, M.B. and Strephens, J.A. (1998) Gulf stream shifts following ENSO events. *Nature.* **393.**

Trenberth, K.E., Jones, P.D., Ambenje, P., Bojariu, R., Easterling, D., Klein Tank, A., Parker, D., Rahimzadeh, F., Renwick, J.A., Rusticucci, M., Soden B. and Zhai, P. (2007) *Observations: Surface and Atmospheric Climate Change*. In: Climate Change 2007: The Physical Science Basis. Contribution of Working Group I to the Fourth Assessment Report of the Intergovernmental Panel on Climate Change [Solomon, S., D. Qin, M. Manning, Z. Chen, M. Marquis, K.B. Averyt, M. Tignor and H.L. Miller (eds.)].

Trigo, R.M., Valente, M.A., Trigo, I.F., Miranda, P.M.A., Ramos, A.M., Paredes, D., Garcia-Herrera, R. (2008) The Impact of North Atlantic Wind and Cyclone Trends on European Precipitation and Significant Wave Height in the Atlantic, *Annals of the New York Academy of Sciences***. Vol. 1146, suppl. 1,** pp. 212-234**.**

Tucker, M.J. and Pitt, E.G. (2001) *Waves in Ocean Engineering*. p. 521.

Uppala, S.M., Dee, D., Kobayashi, S., Berrisford, P. and Simmons A. (2008) Towards a climate data assimilation system: status update of ERA-Interim. **Newsletter 115** – Spring 2008. ECMWF pp. 12-19.

Uppala, S.M., Kallberg, P.W., Simmons, A.J., Andrae, U., Da Costa Bechtold, V., Fiorino, M., Gibson, J.K., Haseler, J., Hernandez, A., Kelly, G.A., Li, X., Onogi, K., Saarinen, S., Sokka, N., Allan, R.P., Andersson, E., Arpe, K., Balmaseda, M.A., Beljaars, A.C.M., Vande Bergy, L., Bidlot, J., Bormass, N., Caires, S., Chevallier, F., Dethof, A., Dragosavac, M., Fisher, M., Fuentes, M., Hagemann, S., Ho'lm, E., Hoskins, B.J., Isaksen, L., Janssen, P.A.E.M., Jenne, R., McNally, A.P., Mahfour, J-F., Morcrette, J-J., Rayner, N.A., Saunders, R.W., Simon, P., Sterl, A., Trenberth, K.E., Untch, A., Vasiljevic, D., Viterbo, P. and Woollen, J. (2005) The ERA-40 re-analysis. *Quarterly Journal of Royal Meteorological Society*, **131**, pp. 2961-3012.

Visbeck, M. NAO images. Available online from: http://www.ldeo.columbia.edu/NAO. Accessed 29th July 2009.

Wallace, J.M., and Gutzler, D.S. (1981) Teleconnections in the geopotential height field during the Northern hemisphere Winter. *Monthly Weather. Review*., **109**, pp. 784-812.

Wang, X.L., Swail, V.R., Zwiers, F.W., Zhang, X. and Feng, Y. (2009) Detection of external influence on trends of atmospheric storminess and northern ocean waves heights. *Climate Dynamics.* **32.** pp. 189-203.

Wang, X. L., Zwiers, F.W. and Swail, V.R., (2004) North Atlantic Ocean wave climate change scenarios for the twenty-first century, *Journal of Climate*, **17**, pp. 2368–2383.

Wolf, J. and Woolf, D.K. (2006) Waves and climate change in the north-east Atlantic. *Geophysical Research Letters.* **33(L06604)**.

Wolter, K. (1987) The Southern Oscillation in surface circulation and climate over the tropical Atlantic, Eastern Pacific, and Indian Oceans as captured by cluster analysis. *Journal of Climate and Applied Meteorolgy.*, **26**, pp. 540-558.

Wolter, K., and Timlin, M.S. (1993) Monitoring ENSO in COADS with a seasonally adjusted principal component index. *Proc. of the 17th Climate Diagnostics Workshop*, Norman, OK, NOAA/NMC/CAC, NSSL, Oklahoma Clim. Survey, CIMMS and the School of Meteor., Univ. of Oklahoma, pp. 52-57.

Woolf, D.K., Challenor, P.G. and Cotton, P.D. (2002) Variability and predictability of the North Atlantic wave climate. *Journal of Geophysical Research.* **107(C10)**

Woolf, D.K., Cotton, P.D., and Challenor, P.G., (2003) Measurements of the off shore wave climate around the British Isles by satellite altimeter. *Philosophical Transactions of the Royal. Society. London.* A., **361**, pp. 27-31

Wu, A. M., and Hsieh, W. W. (2004) The nonlinear Northern Hemisphere winter atmospheric response to ENSO. *Geophysical Research Letters*, **31, L02203**,

Wyrtki, K. (1975) El Niño—The Dynamic Response of the Equatorial Pacific Ocean to Atmospheric Forcing. *Journal of Physical Oceanography*. **5,** pp. 572-584.

Young, I.R. (1999) An intercomparison of GEOSAT, Topex and ERS-1 measurements of wind speed and wave height, *Ocean Engineering*, **26**, pp. 67 – 81.

Young, I.R. (1999b) seasonal variability of the global ocean wind and wave climate. *International Journal of Climatology*. **19(9).** pp. 931-950.

Appendices

Appendix. 1. Notation

Significant wave height = swh = $4\sqrt{m_o}$

Mean wave period = mwp = Energy period = $T_e = m_{-1} / m_0$

Zero upcrossing period = $T_z = \sqrt{m_o / m_2}$

Mean period = $T_m = m_0 / m_1$

nth moment of the wave power spectral density function S(f). $m_n = \int_0^{f\,\mathrm{lim}} f^n S(f) df$. Where

$f\,\mathrm{lim}$ is the high-frequency cutoff of the measuring device.